Journal of *Marine Science and Engineering*

MDPI

Article

Volumetric Path Planning and Visualization for ROV-Based Forward-Looking Sonar Scanning of 3D Water Areas

Yu-Cheng Chou [1,2,*] and Wei-Shan Chang [1]

[1] Institute of Undersea Technology, National Sun Yat-sen University, Kaohsiung 804201, Taiwan
[2] Marine-Science-Oriented Ocean Technology Implementation Center, National Sun Yat-sen University, Kaohsiung 804201, Taiwan
* Correspondence: ycchou@mail.nsysu.edu.tw; Tel.: +886-7-5252000 (ext. 5288)

Abstract

Remotely operated vehicles (ROVs) equipped with multibeam forward-looking sonar are widely used for underwater object search in environments where visibility is limited. Ensuring complete three-dimensional (3D) scan coverage within a bounded mission duration remains a challenging planning problem due to sonar beam geometry and vehicle motion constraints. This study presents a deterministic, geometry-driven framework for volumetric path planning of ROV-based forward-looking sonar scanning in predefined circular and rectangular underwater volumes. The proposed approach constructs layered planar scan trajectories by explicitly incorporating sonar detection range, horizontal and vertical beamwidths, and scan volume geometry. Mission duration is analytically estimated from path length and vehicle kinematic parameters, enabling systematic comparison among multiple planning strategies. To support qualitative interpretation of scan effectiveness, a distance-based target position certainty metric is introduced and combined with the active sonar equation to estimate likely target locations within the scanned volume. Simulation results under idealized sensing and motion assumptions demonstrate that the corrected zigzag pattern for rectangular scan areas, as well as the corrected zigzag-II and corrected arithmetic spiral-III patterns for circular scan areas, achieve complete volumetric coverage with bounded mission duration and consistent localization performance. The proposed framework provides a transparent analytical baseline for evaluating volumetric scan path planning strategies for forward-looking sonar–equipped ROVs.

Keywords: forward-looking sonar; remotely operated vehicle; target localization; three-dimensional underwater scanning; volumetric path planning

Academic Editor: Weicheng Cui

Received: 29 October 2025
Revised: 6 February 2026
Accepted: 11 February 2026
Published: 27 February 2026

1. Introduction

Unmanned underwater vehicles (UUVs) are generally categorized into remotely operated vehicles (ROVs) and autonomous underwater vehicles (AUVs), each offering distinct operational capabilities. These platforms are widely employed across diverse underwater applications, including scientific research, engineering inspection, civil operations, and national defense. Depending on mission objectives, environmental conditions, and sensing requirements, different UUV configurations are selected, leading to fundamentally different planning, sensing, and operational considerations.

UUV-based operations are particularly valuable in remote, hazardous, or access-limited underwater environments where direct human intervention is impractical or unsafe. In such contexts, the effectiveness of a mission depends not only on vehicle reliability but

also on systematic mission planning, which accounts for sensing geometry, environmental constraints, and limited operational time. As emphasized by Bellingham and Rajan [1], underwater robotic systems are increasingly required to execute structured survey and search tasks with minimal human supervision, motivating the need for transparent and reliable pre-mission planning strategies.

One representative class of underwater missions involves confirming the presence and approximate location of a single moored object, such as a mine, within a designated three-dimensional (3D) underwater volume. In such missions, scan completeness and temporal efficiency are directly governed by the interaction between path planning strategy and sensing modality. Because these objects are often deployed covertly and in isolation to increase detection difficulty, the sensing system must support reliable volumetric scanning, particularly under low-visibility conditions where visual confirmation is infeasible. Common sensing options include underwater cameras, side-scan sonar (SSS), and multibeam imaging sonar configured as forward-looking sonar (FLS). A comparison of these sensor types is summarized in Table 1. While underwater cameras provide high-resolution imagery, their effectiveness is strongly limited by turbidity and lighting; side-scan sonar enables efficient two-dimensional (2D) seafloor coverage but is ineffective for detecting suspended objects or midwater targets; by contrast, forward-looking multibeam sonar provides real-time acoustic imaging of the water column ahead of the vehicle and is capable of detecting mid-column moored objects in turbid or dark environments.

Table 1. Comparison of common sensing modalities for volumetric underwater object search (midwater/moored targets).

Sensor Type	Advantages	Limitations
Underwater camera	− High-resolution visual imagery for object identification − Lightweight and energy-efficient	− Strongly affected by turbidity and lighting conditions − Narrow field of view − Requires artificial lighting in dark or deep waters
Side-scan sonar (SSS)	− Broad lateral seafloor coverage − Effective for detecting objects resting on the bottom	− Provides only 2D imagery − Cannot detect suspended or midwater targets − Subject to shadowing and terrain effects
Multibeam imaging sonar (FLS)	− Real-time 2D acoustic imaging − Operates effectively in turbid or dark environments − Detects suspended or moored objects in front of the vehicle	− Does not generate 3D imagery in real time − May require experienced interpretation − Typically narrower field of view compared to SSS

Accordingly, this study adopts a multibeam imaging sonar configured in a forward-looking orientation as the primary sensing modality. Although such systems do not generate real-time 3D imagery, they enable robust forward-looking detection within a bounded 3D water volume and operate effectively in environments where visibility is constrained. An ROV equipped with this sonar is tasked with performing a complete volumetric scan of a predefined underwater region within a limited mission duration, subject to constraints imposed by sonar beam geometry and vehicle motion characteristics.

To address this problem, this study develops and systematically evaluates multiple volumetric path planning strategies for both cylindrical and rectangular scan volumes. The proposed methods generate layered planar scan trajectories at different depths, explicitly accounting for sonar detection range, horizontal and vertical beamwidths, and the geometric constraints of the scan volume. The resulting trajectories are evaluated in terms of scan completeness, total path length, vertical traversal distance, and estimated mission duration under specified ROV motion constraints.

A variety of studies have investigated underwater path planning strategies for autonomous and remotely operated vehicles, with emphasis on planar coverage, terrain adaptability, control robustness, and execution efficiency.

From a broader robotics perspective, coverage path planning (CPP) has been extensively studied as a fundamental problem involving the systematic traversal of an area or volume to ensure complete sensing or actuation. Galceran and Carreras [2] provided a comprehensive survey of CPP methods, including classical zigzag and spiral patterns, and discussed their application across multiple robotic domains, including AUVs performing imaging and survey tasks. While most surveyed approaches focus on planar coverage, their geometric foundations provide important context for extending coverage concepts to layered three-dimensional scan formulations.

Goh and Fan [3] evaluated classical two-dimensional coverage strategies—including zigzag, inward and outward spirals, and spiral-shift patterns—for AUV operations using the MOOS-IvP framework, and further introduced a current-compensated path-tracking algorithm to improve execution robustness. Their study primarily addressed planar area coverage for sonar-based imaging. In contrast, the present work extends these coverage concepts into a layered three-dimensional formulation designed explicitly for volumetric scanning using forward-looking multibeam sonar.

Cardaillac and Ludvigsen [4] developed a path-following control framework for ROV inspection tasks under maneuvering constraints by integrating Line-of-Sight (LOS) guidance with PID control across four degrees of freedom. Their work focused on close-range waypoint tracking and attitude regulation during inspection maneuvers. By contrast, the present study addresses long-range volumetric scan planning, where trajectory generation is governed primarily by sonar detection geometry rather than local control performance.

Shi and Zhou [5] proposed an intermittent, data-driven coverage path planning (CPP) method for bathymetric mapping with AUVs, in which waypoints are dynamically updated to accommodate terrain complexity and sonar variability. Their approach emphasizes adaptive coverage of irregular seabeds during mission execution. In contrast, the present work focuses on pre-mission planning to ensure complete scan coverage of a predefined and bounded three-dimensional water volume.

Recent research has expanded toward three-dimensional scanning, real-time detection, and uncertainty-aware planning for underwater vehicles. Wang et al. [6] introduced a constant-depth AUV survey method for unfamiliar waters by integrating sonar safety margins and survey efficiency through a vertical constraint model. While their work focused on adapting trajectories to unknown bathymetry, the present study assumes a pre-characterized scan volume and emphasizes deterministic scan logic derived from sonar beam geometry. Tang et al. [7] addressed real-time target detection using side-scan sonar by combining deep learning with onboard data processing to overcome communication limitations. By contrast, the present work supports indirect target detection by ensuring complete volumetric scan coverage prior to deployment. Masmitja et al. [8] applied reinforcement learning to optimize range-only localization paths near targets, demonstrating improved performance over traditional solutions. In comparison, the present study adopts fixed, geometry-driven planning strategies to guarantee consistent coverage

within a bounded mission duration. Mane et al. [9] proposed a 2.5D sonar-based obstacle avoidance method by dynamically pivoting a two-dimensional multibeam sensor to enable navigation in cluttered three-dimensional environments. While their approach prioritizes reactive safety, the present work emphasizes structured scan path generation to achieve full-area volumetric coverage.

SLAM-based approaches have primarily focused on localization and mapping during sonar-guided operations. Cheng et al. [10] implemented a multibeam sonar SLAM system based on Rao-Blackwellized particle filtering and sparse point cloud conversion, enabling efficient mapping under sensor bandwidth constraints. Zhang et al. [11] presented a side-scan sonar SLAM framework that reduces localization drift through keypoint matching and pose optimization. While these methods improve trajectory estimation and map quality during or after mission execution, the present study incorporates sonar detection geometry directly into the pre-mission planning stage to ensure guaranteed spatial coverage of the scan volume.

Deterministic underwater survey strategies have also been demonstrated in large-scale field deployments, where structured path planning is critical for achieving reliable coverage under limited endurance. Yoerger et al. [12] reported autonomous deep-sea survey missions using layered and nested trajectory designs to systematically cover near-bottom regions. Although their work focused on terrain-following bathymetric surveys, it highlights the effectiveness of geometry-driven, pre-planned trajectories for ensuring coverage in three-dimensional underwater environments.

In contrast to prior efforts that emphasize online adaptability, target localization, or reactive obstacle avoidance, the present study focuses on achieving complete three-dimensional volumetric scan coverage through the formulation of layered path planning strategies derived from the detection range and beam geometry of a multibeam forward-looking sonar. Rather than pursuing real-time three-dimensional reconstruction or adaptive decision-making during mission execution, the proposed approach is optimized for systematic target search within a predefined underwater volume. The objective is to guarantee full spatial coverage within a bounded mission duration, while enabling the reliable detection of a single moored object.

All simulations presented in this study assume an ideal, disturbance-free underwater environment in which the ROV follows the predefined trajectories without deviation. This assumption is adopted intentionally to isolate and evaluate the geometric efficiency and coverage characteristics of different path planning strategies, independent of environmental disturbances, sensing uncertainty, or control performance. The proposed framework is therefore intended to serve as a baseline reference for systematic comparison under controlled conditions rather than as a direct prediction of field performance.

This work builds upon our prior UT2025 conference paper [13] by providing substantially expanded algorithmic detail, broader volumetric scan scenarios, and enhanced three-dimensional visualization and analysis of scan coverage and target position certainty through a customized simulation interface.

2. Methods and Simulation Setup

2.1. System Configuration and Operational Parameters

This section outlines the representative hardware configuration and mission parameters used to inform the volumetric scan planning process, including the specifications of the forward-looking sonar, assumed ROV operational capabilities, and the geometry of the designated scan area. These parameters are selected to support systematic evaluation of scan coverage and mission duration rather than to prescribe a specific vehicle implementation.

2.1.1. Sonar Specification

This study adopts representative sonar specifications based on the Oculus M750d multibeam imaging sonar (Blueprint Subsea Ltd., Cumbria, UK) [14], which is used as an example of a commercially available forward-looking multibeam sonar. The Oculus M750d operates at selectable frequencies of 720 kHz or 1200 kHz. At 720 kHz, it provides a detection range of 0.1 to 120 m, with a horizontal beamwidth of 130° and a vertical beamwidth of 20°. At 1200 kHz, the detection range is reduced to 0.1 to 40 m, with a horizontal beamwidth of 80° and a vertical beamwidth of 12°.

In this study, the sonar scanning geometry is analyzed using parameters corresponding to the 720 kHz setting, including a horizontal beamwidth of 130°, a vertical beamwidth of 20°, and a detection range (R) of 100 m. A down-tilt angle (ψ) of 15° is adopted as a representative mounting configuration consistent with manufacturer recommendations for forward-looking seabed observation, providing a wide insonified region in front of the vehicle. From the top view (Figure 1b), the sonar generates a sector-shaped scanning area with a chord length (α) of 181.3 m, as calculated using Equation (1). From the side view (Figure 1c), the sonar forms a corresponding vertical sector yielding a sector height (β) of 42.26 m, as calculated using Equation (2). The chord length (α) defines the lateral coverage within a single horizontal scan layer, while the sector height (β) determines the number of vertical scan layers required to achieve complete volumetric coverage of the scan area.

$$\alpha = 2R\sin\left(\frac{\theta}{2}\right) \tag{1}$$

$$\beta = 2R\sin\left(\frac{\phi}{2} + \psi\right) \tag{2}$$

where α is the top-view scan sector chord length; β is the side-view scan sector height; R is the sonar detection range; θ is the horizontal beamwidth; ϕ is the vertical beamwidth; ψ is the sonar tilt angle.

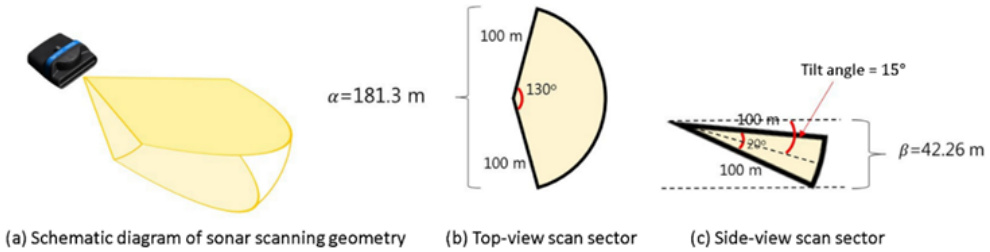

Figure 1. Sonar scanning parameters at 100 m detection range with the multibeam imaging sonar.

2.1.2. ROV Specifications

This study adopts representative ROV specifications based on the Seascan-M ROV (Exail Technologies, Paris, France) [15], which is used as an example of a work-class inspection ROV suitable for mine identification and underwater survey missions. Its motion performance characteristics are summarized in Table 2, including a rated speed range of 0 to 4 knots and a maximum speed of 5 knots. The specified maximum operational endurance of 3 h is referenced to inform mission time assumptions in the simulation.

Table 2. Motion performance characteristics of the Seascan-M ROV [12].

Parameter	Specification
Endurance	Up to 3 h
Max. speed	5 knots
Nominal speed	0 to 4 knots
Max operational depth	300 m
Operational range	Up to 1500 m

Based on these representative specifications, the ROV motion parameters assumed in this study include a constant cruising speed of 1.5 m/s, a constant diving speed of 0.25 m/s, and a constant turning rate of 10°/s. The mission time limit is set to 1.5 h, corresponding to a conservative fraction of the referenced endurance, in order to maintain an operational margin for contingencies such as maneuvering, recovery, or unexpected delays. This assumption reflects a representative planning constraint rather than a universal limitation applicable to all ROV platforms.

2.1.3. Scan Area Selection and Dimensions

In mine scanning and similar survey missions, the selection of an appropriate planar scan area shape directly influences scan path structure, coverage regularity, and navigation safety. Circular and rectangular scan areas are among the most commonly adopted geometries, particularly for sonar-based search operations. Each shape imposes different geometric constraints on path planning and volumetric coverage, motivating their separate consideration in this study.

A circular scan area enables radially symmetric coverage centered about a reference point, which simplifies the generation of layered scan paths and results in uniform angular coverage. From a planning perspective, this geometry is well suited to systematic outward or inward traversal patterns and provides consistent overlap characteristics when projected into a three-dimensional cylindrical scan volume.

A rectangular scan area supports grid-based traversal patterns that are well suited to elongated or structured regions. From a planning standpoint, this geometry facilitates uniform line spacing, predictable turning behavior, and straightforward extension into a three-dimensional cuboid scan volume through stacked horizontal layers.

In this study, the corresponding three-dimensional scan volumes are defined as follows:

- For a circular planar scan area, a cylindrical volume is defined with a diameter of 400 m and a depth of 50 m.
- For a rectangular planar scan area, a cuboid volume is defined with a length of 400 m, a width of 400 m, and a depth of 50 m.

2.2. Volumetric Path Planning Methods

This section introduces five representative path planning patterns for volumetric scanning, including the zigzag, inward spiral, outward spiral, spiral shift, arithmetic spiral-I, and arithmetic spiral-II patterns. The zigzag, inward spiral, outward spiral, and spiral shift patterns are applicable to both circular and rectangular scan areas and are illustrated here using circular scan geometries for clarity. The arithmetic spiral-I and arithmetic spiral-II patterns are designed specifically for circular scan areas. All patterns are formulated to support complete three-dimensional scan coverage through layered planar trajectories. Each method is subsequently simulated and evaluated under identical assumptions to enable systematic comparison.

2.2.1. Zigzag Pattern

Step 1: Determine the number of top-view scan sectors required to cover a single horizontal scan layer. As an illustrative example, a circular scan area with a radius of 200 m is considered, together with a sonar detection range of 100 m, a horizontal beamwidth of 130°, and a vertical beamwidth of 20°. Under these parameters, the chord length (α) of a top-view scan sector is 181.3 m, while the corresponding side-view scan sector height (β) is 42.26 m. Using Equation (3), the number of top-view scan sectors required to fully cover the circular scan area is calculated as three, as illustrated in Figure 2.

$$n_1 = \left\lceil \frac{2R}{\alpha} \right\rceil \tag{3}$$

where n_1 denotes the number of top-view scan sectors required to cover the circular scan area, R is the sonar detection range, α is the chord length of the top-view scan sector, and $\lceil \cdot \rceil$ represents the ceiling function.

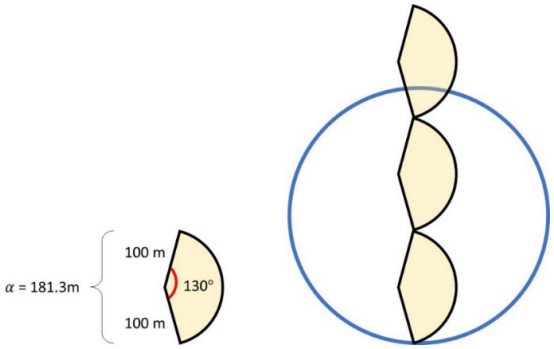

Figure 2. Coverage of a circular scan area with a 400 m diameter using three top-view scan sectors.

Step 2: Compute the overlap length between adjacent top-view scan sectors to achieve uniform overlap distribution. As shown in Equation (4), the combined length of three top-view scan sectors under the example parameters is 543.9 m, exceeding the scan diameter of 400 m by 143.9 m. Because two overlap regions exist between three adjacent sectors, the excess length is evenly distributed, resulting in an average overlap length of 71.95 m, as illustrated in Figure 3.

$$\gamma_1 = \frac{\alpha n_1 - 2R}{n_1 - 1} \tag{4}$$

where γ_1 denotes the overlap length between adjacent top-view scan sectors, α is the chord length of a top-view scan sector, n_1 is the number of required scan sectors, and R is the sonar detection range.

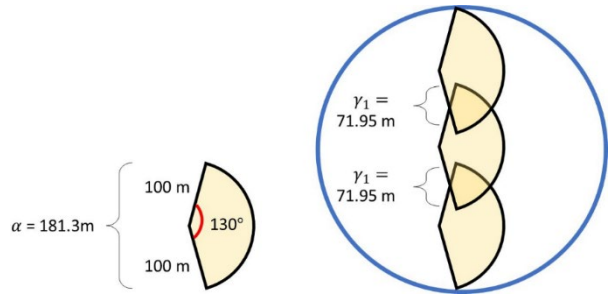

Figure 3. Calculation of the overlap length between top-view scan sectors.

Step 3: Generate horizontal scan paths by positioning them along the centerlines of the top-view scan sectors, and compute the intersection points between each horizontal path

and the scan area boundary. Using the three sector centerlines in the illustrative example, three horizontal scan paths and their corresponding endpoints are obtained, as shown in Figure 4.

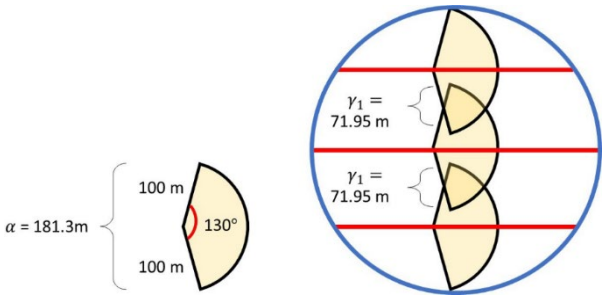

Figure 4. Horizontal paths (red lines) generated based on the centers of the top-view scan sectors.

Step 4: Connect the horizontal scan paths according to the zigzag traversal rule. Specifically, the right endpoint of the first (bottom-most) horizontal path is connected to the right endpoint of the second path, followed by a connection between the left endpoints of the second and third paths. By alternately connecting endpoints on opposite sides, a continuous zigzag trajectory is formed, starting from the initial point and terminating at the final point, as illustrated in Figure 5.

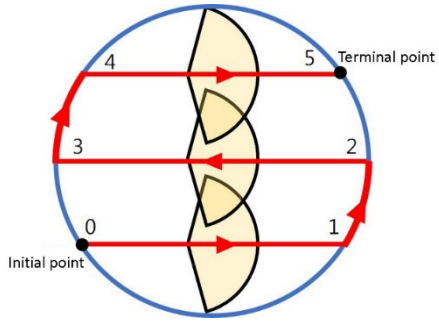

Figure 5. Result of zigzag path planning.

Step 5: Determine the number of vertical scanning layers required to cover the total scan depth using the side-view scan sector height (β), as expressed in Equation (5). For a scanning depth of 100 m under the example parameters, three vertical scanning layers are required, as illustrated in Figure 6.

$$n_2 = \left\lceil \frac{Depth}{\beta} \right\rceil \tag{5}$$

where n_2 denotes the number of vertical scan layers required to cover the scanning depth, $Depth$ is the total scanning depth, and β is the height of the side-view scan sector.

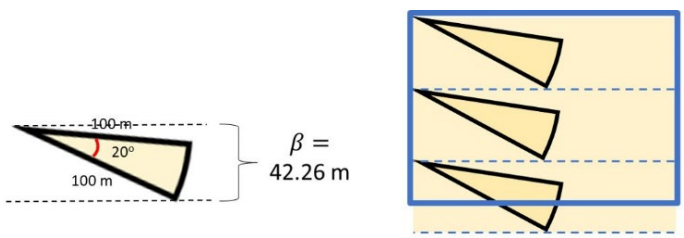

Figure 6. Three vertical scan layers for a scanning depth of 100 m.

Step 6: Compute the overlap length between adjacent side-view scan sectors to ensure uniform vertical overlap, as described in Equation (6). In the illustrative example, the combined height of three side-view scan sectors is 126.78 m, exceeding the scan depth of 100 m by 26.78 m. Because two overlap regions exist, the excess height is evenly distributed, yielding an average overlap length of 13.39 m, as illustrated in Figure 7.

$$\gamma_2 = \frac{\beta n_2 - Depth}{n_2 - 1} \tag{6}$$

where γ_2 denotes the overlap length between adjacent side-view scan sectors, β is the height of a side-view scan sector, n_2 is the number of vertical scan layers, and $Depth$ is the scanning depth.

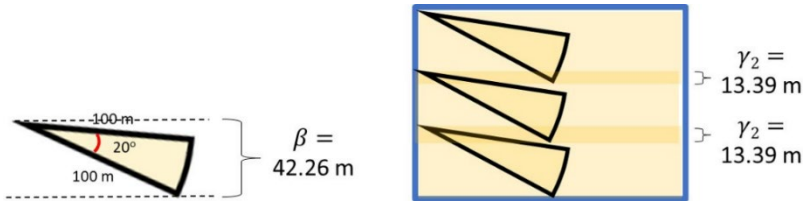

Figure 7. Uniform vertical overlap (γ_2) between adjacent scan layers for a scanning depth of 100 m.

2.2.2. Inward/Outward Spiral Pattern

The inward and outward spiral patterns differ only in their traversal direction and the corresponding selection of initial and terminal points. In the inward spiral pattern, the scan trajectory progresses from the outer boundary toward the center of the scan area, whereas in the outward spiral pattern the trajectory proceeds from the center toward the outer boundary. Both patterns employ the same geometric planning procedure described in Section 2.2.1, with the only modification relative to the zigzag pattern occurring in the path-connection rule of Step 4; all other steps remain identical.

As illustrated in Figure 8, consider the case in which three horizontal scan paths are generated. For the inward spiral pattern, the right endpoint of the first (bottom-most) horizontal path is connected to the right endpoint of the third (top-most) path. The trajectory then continues by connecting the left endpoint of the third path to the left endpoint of the second path. In this configuration, the initial point is located on the first horizontal path, and the terminal point is located on the third horizontal path. Following this ordered sequence of endpoint connections produces a continuous inward spiral trajectory, processing from the outer boundary toward the center of the scan area.

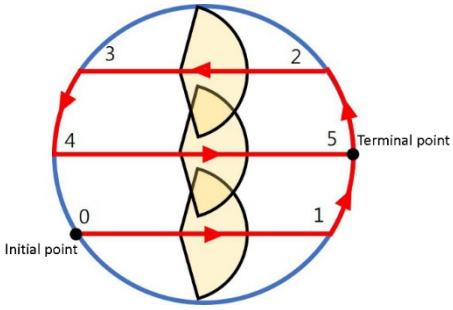

Figure 8. Result of inward spiral path planning.

As shown in Figure 9, the outward spiral pattern follows the same geometric construction as the inward spiral, but with the traversal direction reversed. The right endpoint of the first (bottom-most) horizontal path is connected to the right endpoint of the third path,

followed by a connection between the left endpoints of the third and second paths. In this case, the initial point is located closer to the center of the scan area, and the terminal point lies near the outer boundary. This connection sequence yields a continuous outward spiral trajectory extending from the center toward the periphery of the scan area.

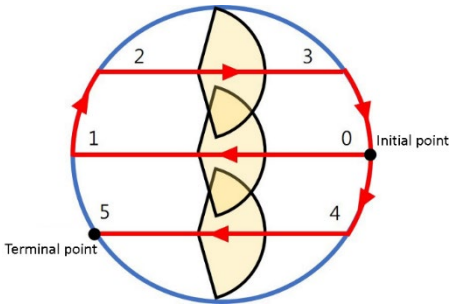

Figure 9. Result of outward spiral path planning.

2.2.3. Spiral Shift Pattern

The spiral shift planning method differs from the zigzag planning method only in the path-connection rule applied in Step 4; all other geometric planning steps remain identical. As illustrated in Figure 10, consider the case in which four horizontal scan paths are generated. The spiral shift trajectory is formed by alternately connecting endpoints of non-adjacent horizontal paths, producing a gradual lateral shift in the traversal direction between successive layers. In this configuration, the initial point is located on the first (bottom-most) horizontal path, while the terminal point lies on the fourth (top-most) horizontal path. Following the prescribed endpoint-connection sequence yields a continuous spiral-shift trajectory spanning the full planar scan area.

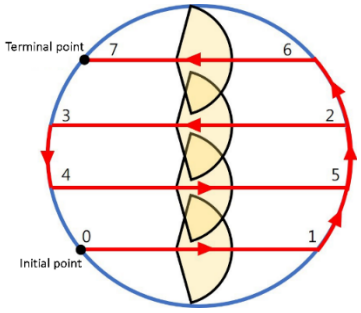

Figure 10. Result of spiral shift path planning.

2.2.4. Arithmetic Spiral-I Pattern for Circular Scan Areas

Step 1: Determine the number of top-view scan sectors required to cover a single horizontal scan layer.

Step 2: Compute the overlap length between adjacent top-view scan sectors to ensure uniform coverage.

These two steps are identical to those used in the previously described path planning methods.

Step 3: Select the appropriate planning strategy based on the number of top-view scan sectors (n_1) required to cover the scan radius.

- When $n_1 = 2$, the trajectory advances to the center of the first (bottom-most) scan sector and then follows a circular path to cover the entire planar layer, as illustrated in Figure 11.

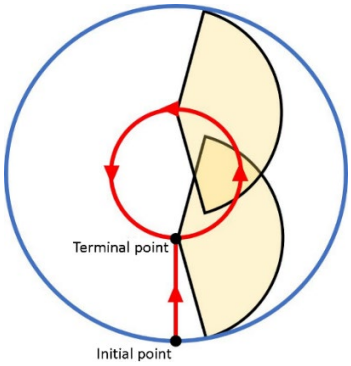

Figure 11. Arithmetic spiral-I pattern when the number of top-view scan sectors equals 2.

- When $n_1 > 2$, an arithmetic spiral trajectory is generated using the centers of the top-view scan sectors as reference points, as illustrated in Figure 12.

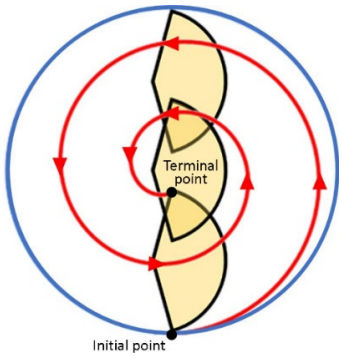

Figure 12. Arithmetic spiral-I pattern when the number of top-view scan sectors is greater than 2.

Step 4: Determine the number of vertical scanning layers required using the side-view scan sector height (β) and the total scanning depth.
Step 5: Compute the overlap length between adjacent side-view scan sectors to ensure uniform vertical coverage.

These steps are identical to Steps 5 and 6 described for the previous path planning methods.

2.2.5. Arithmetic Spiral-II Pattern for Circular Scan Areas

The arithmetic spiral-II planning method is an extension of the arithmetic spiral-I method, intended for cases in which the number of top-view scan sectors (n_1) exceeds two. As the number of spiral loops increases in the arithmetic spiral-I pattern, the degree of path overlap within the scan area also increases. The arithmetic spiral-II pattern is designed to reduce redundant overlap while preserving full planar coverage, thereby reducing the total scan path length and associated mission duration.

- Case 1: $n_1 > 2$ and odd.
  The corresponding planning procedure is illustrated in Figure 13. In this example, $n_1 = 5$, and the arithmetic spiral-I method generates four spiral loops. The arithmetic spiral-II pattern is constructed by modifying the arithmetic spiral-I trajectory according to the following steps:
  1. Retain all odd-numbered spiral loops.
  2. Replace each even-numbered spiral loop by directly connecting its start and end points with a straight-line segment.
  3. Generate a final circular trajectory whose radius is defined by the distance from the scan area center to the endpoint of the outermost retained spiral loop.

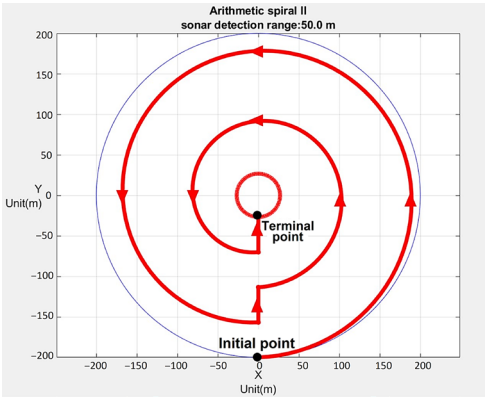

Figure 13. Arithmetic spiral-II pattern for $n_1 > 2$ and odd.

- Case 2: $n_1 > 2$ and even.
  The corresponding planning procedure is illustrated in Figure 14. In this example, $n_1 = 4$, and the arithmetic spiral-I method generates three spiral loops. The arithmetic spiral-II pattern is obtained by:
  1. Retaining all odd-numbered spiral loops.
  2. Replacing the single even-numbered spiral loop by directly connecting its start and end points with a straight-line segment.

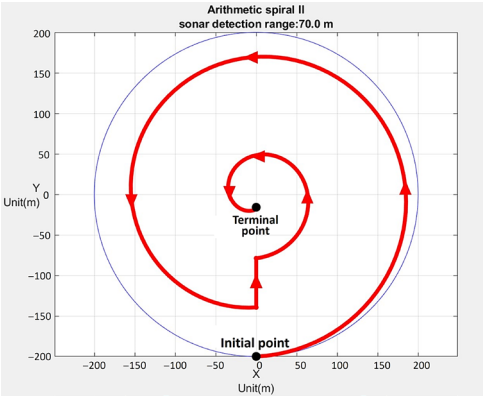

Figure 14. Arithmetic spiral-II pattern for $n_1 > 2$ and even.

2.3. Analytical Estimation of Path Length and Mission Duration

This section outlines the procedures used to estimate the total path length and mission duration based on the planned scan trajectory and ROV motion parameters.

2.3.1. Total Path Length Calculation

In this study, the total path length is calculated by first determining the path length on a single planar layer, then multiplying it by the number of scanning layers, and finally adding the descent distance of the vehicle. For the zigzag, inward spiral, outward spiral, and spiral shift path planning methods, the path length on a single planar layer is computed as the sum of the lengths of all horizontal scan paths and their corresponding connecting segments. For the arithmetic spiral-I and arithmetic spiral-II methods, the spiral path on a single planar layer is approximated by dividing it into a series of small straight-line segments, and the total path length is obtained by summing the lengths of these segments. Additionally, the descent distance is defined as the scanning depth minus the effective vertical coverage of the final scanning layer. As illustrated in Figure 15, for a scan area with a total depth of 100 m and a final layer height of β = 42.26 m, the descent distance is calculated as 57.74 m.

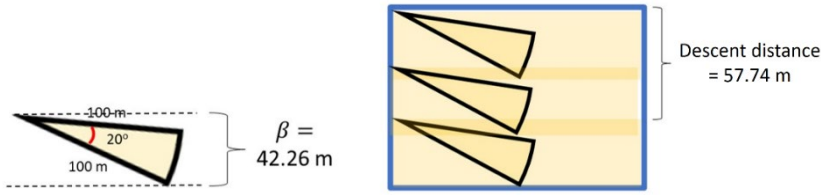

Figure 15. Calculation of descent distance for a scan area with a depth of 100 m.

2.3.2. Total Mission Duration Calculation

In this study, the total mission duration is calculated by first determining the time required to complete the scan path on a single planar layer, then multiplying it by the number of scanning layers, and finally adding the time required for vehicle descent.

For the zigzag, inward spiral, outward spiral, and spiral shift path planning methods, the duration for completing a single planar path is calculated by dividing the total path length on that layer by the vehicle's cruising speed, and adding the time required for vehicle turns. The vehicle turning angle is computed based on the slope between two adjacent path segments. As illustrated in Figure 16, the turning angle (θ_r), indicated by the yellow arc, is calculated using Equation (7).

$$\theta_r = \tan^{-1}\left(\left|\frac{m_1 - m_2}{1 + m_1 \cdot m_2}\right|\right) \tag{7}$$

where θ_r is the turning angle, and m_1 and m_2 are the slopes of two adjacent path segments.

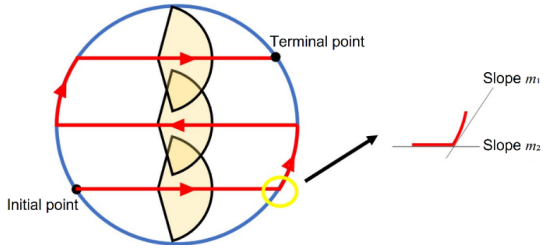

Figure 16. Calculation of vehicle turning angle.

For the arithmetic spiral-I path planning method, the duration of a single planar path is obtained by dividing the total path length by the vehicle's cruising speed. For the arithmetic spiral-II method, the total time is calculated as the sum of the time required to complete the planar path (path length divided by cruising speed) and the time needed for vehicle turns along the connecting segments. These estimates assume idealized vehicle motion and are intended to provide consistent comparative metrics across different path planning patterns.

2.4. Graphical User Interface and Simulation Framework

This section presents a visualization and simulation framework developed to support the systematic configuration and execution of volumetric scan path planning strategies. Specifically, a graphical user interface (GUI) was developed in MATLAB (R2023b) as an analysis and visualization tool for evaluating volumetric scan path planning strategies (Figure 17). The interface enables systematic configuration of scan geometry, sonar detection parameters, and vehicle kinematic constraints, and applies these inputs consistently across different planning methods. Based on the specified parameters, the framework generates candidate scan trajectories and computes associated evaluation metrics, including the number of scan layers, total path length, and estimated mission duration. These outputs

are used to support quantitative comparison of planning strategies under controlled and repeatable conditions, rather than to provide real-time mission execution guidance.

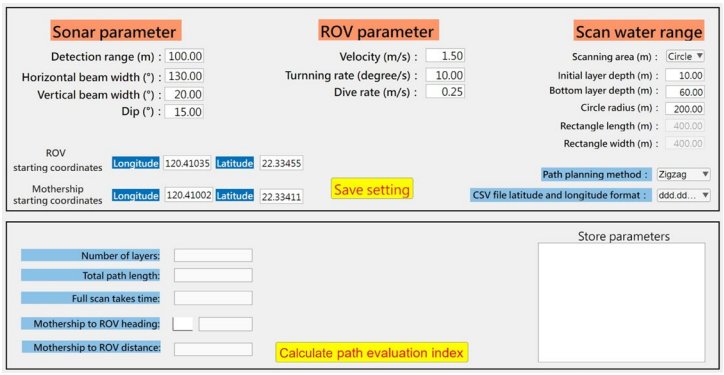

Figure 17. GUI layout showing user input fields and path planning visualization interface.

In addition to local planar visualization, the framework supports conversion of planned trajectories into waypoint sequences referenced to geographic coordinates (WGS84). As illustrated in Figure 18, the resulting paths can be overlaid on nautical charts to verify geometric consistency and spatial feasibility of the planned scan patterns when mapped onto real-world coordinate systems. This visualization is intended to demonstrate coordinate transformation and spatial referencing capability, rather than to represent experimental deployment or field validation.

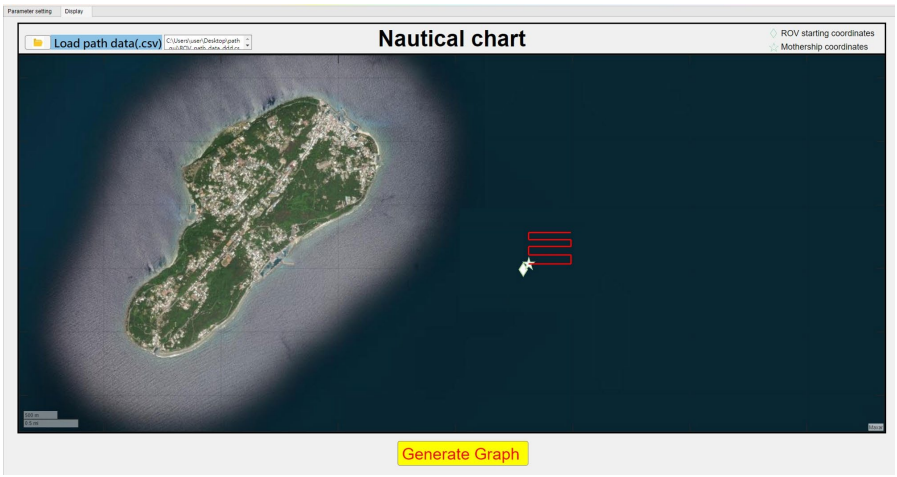

Figure 18. Zigzag waypoint path for a rectangular scan area overlaid on a sea chart near Liuqiu Island.

2.5. ROV Path Following Simulation and Sonar Modeling

To verify the geometric feasibility and coverage characteristics of the proposed path planning algorithms, an OpenGL-based simulation and visualization environment was developed using OpenGL 4.6. The simulation models an ROV equipped with a multibeam forward-looking sonar executing predefined scan trajectories across multiple depth layers. At each layer, the ROV follows the planned path, descends to the starting point of the next layer, and repeats the process until the entire three-dimensional scan volume is traversed. The simulation intentionally excludes vehicle dynamics and feedback control, and instead assumes idealized path following without deviation. This design choice is consistent with the methodological scope of the study, which focuses on evaluating geometric coverage and scan completeness rather than closed-loop control performance. A single stationary target point is placed within each scan volume to support visual interpretation of sonar coverage

and target observability. This section introduces the simulation framework and sonar modeling components used in subsequent analyses. Simulation results and comparative performance evaluations are presented in Section 3.

2.5.1. Target Position Certainty

In this study, target position certainty is defined as a deterministic function of sonar signal travel distance under idealized sensing conditions. As the acoustic wavefront propagates outward from the sonar, the covered area increases with distance, leading to a corresponding increase in the spatial region within which a detected target may be located. As illustrated in Figure 19, the coverage area expands proportionally to the square of the sound travel distance, as expressed in Equation (8). Consequently, greater propagation distance implies increased spatial ambiguity and reduced certainty in estimating the precise target position.

$$\text{Target position certainty} = \left(1 - \frac{r^2}{r_{max}^2}\right) \times 100\% \tag{8}$$

where r is the sound travel distance, which must not exceed the specified sonar detection range; r_{max} is the allowable maximum detection range of the sonar. This metric does not represent a probabilistic detection likelihood, but rather a normalized geometric indicator of spatial uncertainty that decreases monotonically with increasing sound travel distance.

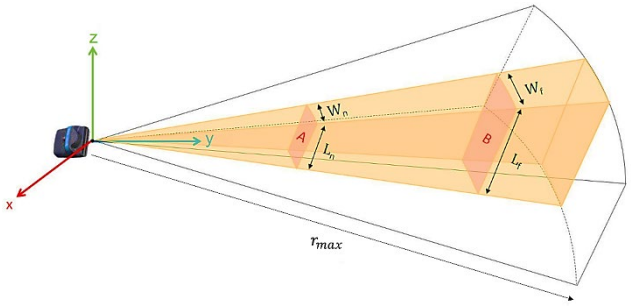

Figure 19. Expansion of sound wave coverage area as a function of travel distance.

To facilitate qualitative interpretation of this metric, a color mapping scheme is employed to visualize target position certainty within the simulation environment. As shown in Figure 20, higher certainty values are indicated by warm colors, with dark red representing the maximum value. This mapping is applied in the visualization interface based on the distance between the target location and the multibeam forward-looking sonar. The resulting display provides an intuitive means of identifying regions of strong and weak geometric observability, thereby supporting visual assessment of volumetric scan coverage rather than serving as a quantitative detection performance measure.

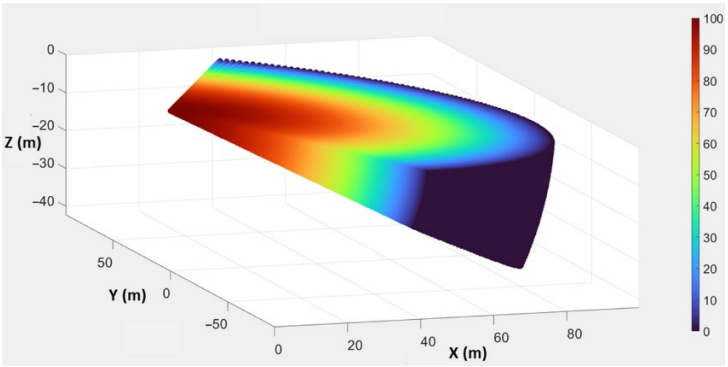

Figure 20. Color-coded distribution of target position certainty based on distance from the multibeam forward-looking sonar.

2.5.2. Three-Dimensional Color Mapping in the ROV Animation Interface

To visualize sonar coverage and target position certainty in three dimensions, this study implements a color mapping approach within the ROV animation interface. The 3D scan area—measuring 400 m in length, 400 m in width, and 50 m in depth—is divided into 64,000 uniform cubes, each with dimensions of 5 m × 5 m × 5 m. The certainty of target detection in each cube is computed based on its spatial relationship with the ROV and the sonar's scanning geometry.

- Step 1: For each cube, its position is first transformed into the ROV's body-fixed reference frame. This process involves two steps. First, the origin of the earth-fixed reference frame is translated to align with the origin of the ROV's body-fixed reference frame. Second, a rotation matrix representing the ROV's orientation—defined by roll (ϕ), pitch (θ), and yaw (ψ) —is applied to convert the cube's coordinates from the translated earth-fixed frame into the ROV's body-fixed frame. This transformation is described by Equation (9).

$$\begin{bmatrix} X' \\ Y' \\ Z' \end{bmatrix} = \begin{bmatrix} \cos\theta\cos\psi & \cos\theta\sin\psi & -\sin\theta \\ \sin\phi\sin\theta\cos\psi - \cos\phi\sin\psi & \sin\phi\sin\theta\sin\psi + \cos\phi\cos\psi & \sin\phi\cos\theta \\ \cos\phi\sin\theta\cos\psi + \sin\phi\sin\psi & \cos\phi\sin\theta\sin\psi - \sin\phi\cos\psi & \cos\phi\cos\theta \end{bmatrix} \begin{bmatrix} X_A - X_R \\ Y_A - Y_R \\ Z_A - Z_R \end{bmatrix} \quad (9)$$

where (X', Y', Z') are coordinates of the cube in the ROV's body-fixed reference frame; (X_A, Y_A, Z_A) and (X_R, Y_R, Z_R) are coordinates of the cube and the ROV in the earth-fixed reference frame, respectively. The coordinates of the cube in the ROV's body-fixed reference frame are then transformed into the sonar look-direction coordinate frame.

- Step 2: The coordinates of each cube are converted to spherical coordinates. Specifically, the radial distance (R), horizontal angle (ω), and vertical angle (γ) are calculated using Equations (10)–(12), as illustrated in Figure 21.

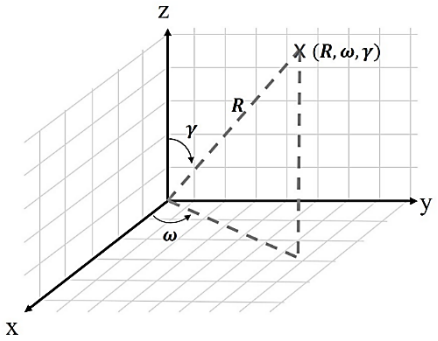

Figure 21. Spherical coordinate system used to represent the relative position between the ROV and each cube.

$$R = \sqrt{X^2 + Y^2 + Z^2} \quad (10)$$

$$\gamma = \cos^{-1}\left(\frac{Z}{\sqrt{X^2 + Y^2 + Z^2}}\right) \quad (11)$$

$$\omega = \tan^{-1}\frac{Y}{X} \quad (12)$$

- Step 3: Each cube is evaluated to determine whether it lies within the sonar's scanning volume. For instance, if the sonar has a detection range of 100 m, a horizontal beamwidth of 130°, and a vertical beamwidth of 20°, then a cube satisfies the sonar

coverage conditions if: (a) $R \leq 100$ m; (b) $80^\circ \leq \gamma \leq 100^\circ$ (i.e., a 20° vertical fan centered at 90° downward); (c) $-65^\circ \leq \omega \leq 65^\circ$ (i.e., a 130° horizontal fan centered forward). If these conditions are met, the cube is considered to be within the sonar's field of view. A certainty value is then computed based on the distance R, and a corresponding color—based on the mapping previously introduced—is applied. If the cube already has an assigned certainty value from a previous scan, the higher value is retained to reflect the most confident observation.

2.5.3. Active Sonar Equation

The active sonar equation describes the quantitative relationship among acoustic parameters involved in the transmission and reception processes of an active sonar system. It is derived based on the assumption that the sonar source behaves as a spherical radiator (i.e., a point source), meaning that sound energy propagates uniformly in all directions from the source.

As the propagation distance increases, the sound pressure level decreases due to energy spreading and attenuation. This phenomenon is governed by the principle of spherical spreading, which forms the basis for the active sonar equation expressed in Equation (13). Echo level (EL) represents the intensity of the reflected sound wave received by the sonar, typically measured in decibels (dB). Source level (SL) is the initial intensity of the emitted sound wave, also in decibels. Transmission loss (TL) quantifies the energy reduction during sound wave propagation. Since the signal travels to the target and then returns, the total transmission loss is doubled. TL is calculated using Equation (14) and increases with the propagation distance. Target strength (TS) characterizes the reflective capability of the target and is positively correlated with the object's physical size—specifically, its radius. TS is given by Equation (15) and is also expressed in decibels. These relationships collectively define the performance of active sonar systems in detecting underwater objects and explain why both target distance and target size influence detectability, even under idealized sensing assumptions.

$$EL = SL - (2TL) + TS \tag{13}$$

$$TL = 10\log\left(\frac{r^2}{r_0^2}\right) \tag{14}$$

$$TS = 10\log\left(\frac{a^2}{4}\right) \tag{15}$$

where r is the sonar propagation distance; r_0 is the reference distance from the sonar (1 m); a is the radius of the target object.

2.5.4. Suspected Target Distribution in the ROV Animation Interface

This section describes the integration of target position certainty and the active sonar equation to estimate and visualize suspected target locations in the ROV animation interface. When a target is located within the sonar scanning area, its possible position is inferred and marked based on acoustic feedback and spatial coverage. The weight value at each suspected location is calculated as the product of the echo level (EL), as defined in Equation (13), and the target position certainty, as defined in Equation (8). The magnitude of this weight value indicates the likelihood of the target's presence at a given location.

- Determining Target Inclusion Within the Sonar Scanning Area
  Step 1: Convert the global coordinates of the target into the ROV's body-fixed reference frame. This is done by translating the origin of the earth-fixed frame to align with the ROV's position and applying a rotation matrix based on the ROV's orientation (roll ϕ, pitch θ, yaw ψ), as described in Equation (16).

$$\begin{bmatrix} X' \\ Y' \\ Z' \end{bmatrix} = \begin{bmatrix} \cos\theta\cos\psi & \cos\theta\sin\psi & -\sin\theta \\ \sin\phi\sin\theta\cos\psi - \cos\phi\sin\psi & \sin\phi\sin\theta\sin\psi + \cos\phi\cos\psi & \sin\phi\cos\theta \\ \cos\phi\sin\theta\cos\psi + \sin\phi\sin\psi & \cos\phi\sin\theta\sin\psi - \sin\phi\cos\psi & \cos\phi\cos\theta \end{bmatrix} \begin{bmatrix} X_M - X_R \\ Y_M - Y_R \\ Z_M - Z_R \end{bmatrix} \quad (16)$$

where (X', Y', Z') are coordinates of the target in the ROV's body-fixed reference frame; (X_M, Y_M, Z_M) and (X_R, Y_R, Z_R) are coordinates of the target and the ROV in the earth-fixed reference frame, respectively. The coordinates of the target in the ROV's body-fixed reference frame are then transformed into the sonar look-direction coordinate frame.

Step 2: Convert the target's coordinates into spherical coordinates to obtain the radial distance (R), horizontal angle (ω), and vertical angle (γ) using Equations (10)–(12).

Step 3: Determine whether the target lies within the sonar's scanning volume. For example, if the sonar detection range is 100 m, with a horizontal beamwidth of 130° and a vertical beamwidth of 20°, the conditions for inclusion are: (1) $R \leq 100$ m; (2) $-65° \leq \omega \leq 65°$; (3) $80° \leq \gamma \leq 100°$. If all conditions are met, the target is considered to fall within the scanning area. However, due to the sonar's limited vertical resolution, it cannot resolve precise positions along the vertical beam axis. Thus, the entire vertical beam range is marked as the suspected target region, as illustrated in Figure 22.

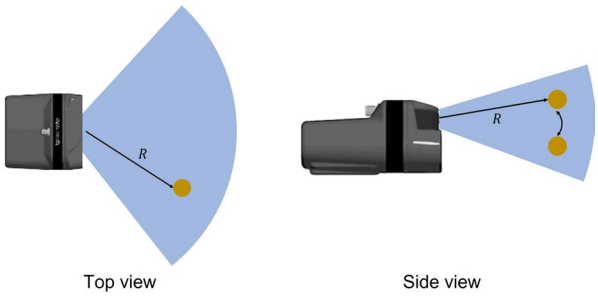

Figure 22. Sonar vertical beam geometry and ambiguity in vertical target resolution.

- Marking Suspected Target Locations

  Step 1: Define the suspected target positions with R and $\omega = 0$ along the sonar's vertical beam angle range. This accounts for vertical ambiguity in sonar detection.

  Step 2: Rotate all suspected target positions by ω about the z-axis, then rotate by 15° about the y-axis.

  Step 3: Transform the suspected target positions from the body-fixed reference frame back to the earth-fixed reference frame, as illustrated in Equation (17).

$$\begin{bmatrix} X_M \\ Y_M \\ Z_M \end{bmatrix} = \begin{bmatrix} \cos\theta\cos\psi & \cos\theta\sin\psi & -\sin\theta \\ \sin\phi\sin\theta\cos\psi - \cos\phi\sin\psi & \sin\phi\sin\theta\sin\psi + \cos\phi\cos\psi & \sin\phi\cos\theta \\ \cos\phi\sin\theta\cos\psi + \sin\phi\sin\psi & \cos\phi\sin\theta\sin\psi - \sin\phi\cos\psi & \cos\phi\cos\theta \end{bmatrix}^T \begin{bmatrix} X' \\ Y' \\ Z' \end{bmatrix} + \begin{bmatrix} X_R \\ Y_R \\ Z_R \end{bmatrix} \quad (17)$$

Step 4: Define a local region measuring 60 m × 60 m × 50 m around the target, and divide it into 1440 cubes of size 5 m × 5 m × 5 m, as shown in Figure 23. For each suspected target location, identify the nearest cube and assign it a weight value, computed as the product of the echo level (EL) and the target position certainty. These weights are visualized in the ROV animation interface using color: the higher the weight, the higher the likelihood of the target's presence. As the ROV navigates through its path, the color scale dynamically adjusts based on the current maximum weight, providing a real-time visualization of suspected target distributions.

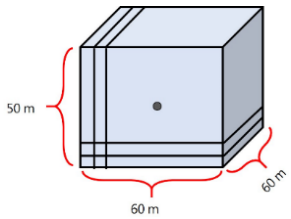

Figure 23. A 60 m × 60 m × 50 m region around the target divided into 1440 cubes of 5 m × 5 m × 5 m.

3. Results and Discussion

3.1. Comparative Evaluation of Path Planning Methods

3.1.1. Comparative Analysis in Circular Scanning Areas

This study compares four path planning methods—zigzag, inward spiral, outward spiral, and spiral shift—under identical parameter settings for circular scan areas. The comparison focuses on total mission duration as a quantitative performance metric derived from the geometric properties of each path pattern and the associated vehicle motion constraints. Under the evaluated conditions, the zigzag pattern exhibits shorter mission durations than the other three methods for the considered circular scan configuration.

Further simulations were conducted to compare the zigzag, arithmetic spiral-I, and arithmetic spiral-II path planning methods under identical geometric and kinematic conditions. The shared simulation parameters include a scan radius of 200 m, scan depth of 50 m, sonar horizontal beamwidth of 130°, vertical beamwidth of 20°, ROV cruising speed of 1.5 m/s, turning rate of 10°/s, and diving speed of 0.25 m/s. The sonar detection range was treated as the independent variable and varied from 10 m to 100 m in increments of 10 m to evaluate its influence on mission duration.

Simulation results, summarized in Table 3, indicate that total mission duration generally decreases as the sonar detection range increases. This trend is primarily attributed to the reduction in the number of required scan layers and horizontal scan paths as detection range increases, leading to shorter overall travel distances. However, several non-monotonic variations are observed. For example, the mission duration for the zigzag pattern increases slightly from 0.67 h to 0.68 h when the detection range increases from 60 m to 70 m. A similar increase is observed for the arithmetic spiral-II pattern within the detection range of 70 m to 80 m.

Table 3. Comparison of zigzag, arithmetic spiral-I, and arithmetic spiral-II patterns.

Sonar Detection Range (m)	Total Mission Duration (Hour)		
	Zigzag	Arithmetic Spiral-I	Arithmetic Spiral-II
100	0.55	0.59	0.52
90	0.54	0.62	0.57
80	0.54	0.66	0.61
70	0.68	0.80	0.58
60	0.67	0.89	0.63
50	1.22	1.65	1.18
40	1.41	2.03	1.31
30	2.41	3.61	2.21
20	5.16	8.12	4.71
10	19.5	32.36	17.81

Among the three methods, the arithmetic spiral-I pattern consistently yields the longest mission durations across the evaluated detection ranges, reflecting its higher degree of path overlap and extended spiral traversal. The zigzag pattern achieves the shortest

mission duration (0.54 h) at detection ranges of 80 m and 90 m, while the arithmetic spiral-II pattern produces the shortest mission durations for most other cases. Both the zigzag and arithmetic spiral-II patterns maintain mission durations below the 1.5 h operational limit when the detection range is between 40 m and 100 m, whereas the arithmetic spiral-I pattern satisfies this constraint only when the detection range exceeds 60 m. To further interpret the observed non-monotonic behavior at specific detection ranges, the underlying path construction logic of the zigzag and arithmetic spiral-II methods is examined in the subsequent sections.

3.1.2. Zigzag-II Pattern

In the original zigzag path planning method, scan sectors are arranged with uniform overlap, and horizontal scan paths are generated from the centers of these sectors (i.e., sonar positions) and connected using an alternating zigzag sequence. While this construction guarantees full planar coverage, a full analysis reveals that, even when the number of scan sectors (n_1) remains constant, the total mission duration does not necessarily decrease monotonically with increasing sonar detection range. This non-monotonic behavior is illustrated in Figure 24.

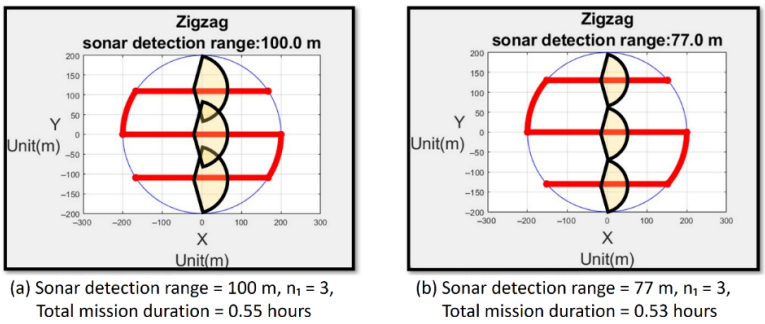

(a) Sonar detection range = 100 m, n_1 = 3, Total mission duration = 0.55 hours

(b) Sonar detection range = 77 m, n_1 = 3, Total mission duration = 0.53 hours

Figure 24. Comparison of total mission duration for zigzag patterns with varying detection ranges and constant n_1.

For example, when the sonar detection range is 100 m, the single-layer path length is 1301.22 m, whereas for a detection range of 77 m, the corresponding path length is reduced to 1290.81 m. To clarify this counterintuitive result, the total path length was decomposed into horizontal scan segments and connecting segments. As the detection range decreases from 100 m to 77 m, the horizontal scan length is reduced from 1069.78 m to 1007.23 m due to shorter effective coverage per sector, while the total length of connecting segments increases from 231.44 m to 283.58 m because of expanded lateral offsets. In this case, the reduction in horizontal path length exceeds the increase in connecting length, resulting in a net decrease in total single-layer path length. The quantitative comparison is summarized in Table 4.

Table 4. Comparison of single-layer path lengths for zigzag patterns with different detection ranges and constant n_1.

Single Planar Layer Path Length	Sonar Detection Range: 100 m	Sonar Detection Range: 77 m	Difference (m)
Total Horizontal Path Length (m)	1069.78	1007.23	+62.55
Total Connecting Path Length (m)	231.44	283.58	−52.14
Total Path Length (m)	1301.22	1290.81	+10.41

To address the irregular trend in mission duration observed in the original zigzag pattern, this study proposes an improved planning strategy referred to as the zigzag-II

pattern. Unlike the original approach, the zigzag-II pattern eliminates intentional overlap between adjacent scan sectors by positioning sector centers further outward, while still maintaining complete planar coverage. This geometric adjustment reduces both horizontal scan length and total single-layer path length, as illustrated in Figure 25. In this representative example, the total single-layer path length is reduced from 1301.22 m for the zigzag pattern to 1218.88 m for the zigzag-II pattern. The same construction principle can be extended to rectangular scan areas to improve scanning efficiency under similar geometric constraints.

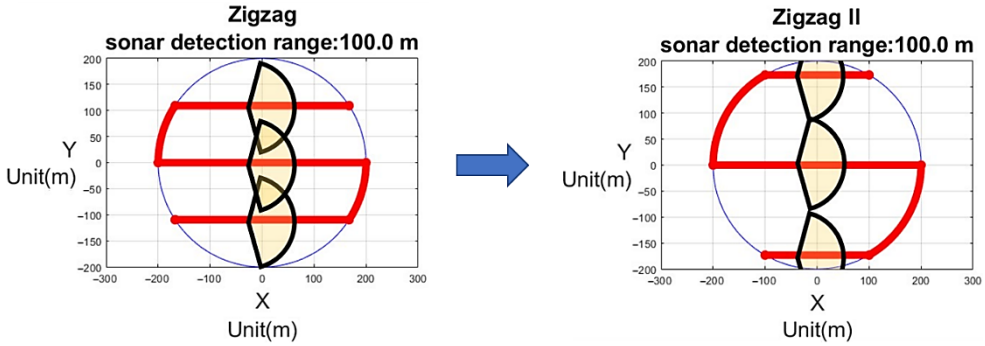

Figure 25. Single-layer path layout of the zigzag-II pattern.

Further simulations demonstrate that the zigzag-II pattern produces a strictly decreasing mission duration as the sonar detection range increases. This behavior contrasts with the non-monotonic trend observed in the original zigzag pattern and indicates improved geometric consistency of the revised path construction. Moreover, for detection ranges between 40 m and 100 m, all mission durations remain below the 1.5 h operational limit. The corresponding simulation results are summarized in Table 5.

Table 5. Simulation results of mission duration for zigzag-II path planning method.

Sonar Detection Range (m)	Total Mission Duration (hour)
100	0.52
90	0.53
80	0.53
70	0.64
60	0.66
50	1.19
40	1.40
30	2.38
20	5.07
10	18.97

3.1.3. Arithmetic Spiral-III Pattern

In the arithmetic spiral-II path planning method, the geometry of the innermost loop depends on whether the number of top-view scan sectors (n_1) is odd or even. When $n_1 > 2$ and odd, the central portion of the path forms a circular loop, whereas for even values of n_1 it forms a spiral. For the odd-n_1 case, the circular loop typically introduces a longer traversal length than a corresponding spiral, which can increase the total mission duration as the sonar detection range varies. To mitigate this effect, an improved planning strategy referred to as the arithmetic spiral-III pattern is proposed. For even values of n_1, the arithmetic spiral-III pattern is identical to the arithmetic spiral-II pattern. For odd values n_1, the innermost circular loop is replaced with a spiral segment, as illustrated in Figure 26, thereby reducing redundant traversal while preserving complete planar coverage.

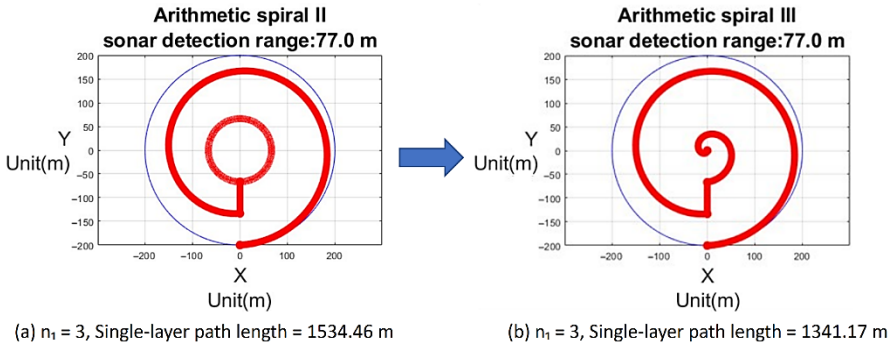

Figure 26. Single-layer path layout for the arithmetic spiral-III pattern.

Simulation results indicate that the arithmetic spiral-III pattern yields a strictly decreasing mission durations as the sonar detection range increases. This behavior demonstrates that the modified inner-loop construction effectively removes the non-monotonic trends observed in the arithmetic spiral-II pattern for odd values of n_1. In addition, for sonar detection ranges between 40 m and 100 m, all mission durations remain below the 1.5 h operational limit. The corresponding results are summarized in Table 6.

Table 6. Simulation results of mission duration for arithmetic the spiral-III path planning method.

Sonar Detection Range (m)	Total Mission Duration (Hour)
100	0.50
90	0.52
80	0.54
70	0.58
60	0.63
50	1.13
40	1.31
30	2.21
20	4.71
10	17.81

3.1.4. Comparative Analysis in Rectangular Scan Areas

This section compares four path planning methods—zigzag, inward spiral, outward spiral, and spiral shift—applied to rectangular scan areas under identical planning parameters. Among the evaluated methods, the zigzag pattern yields the shortest total mission duration and is therefore selected for further analysis. To examine its performance sensitivity, additional simulations were conducted for the zigzag method using a rectangular scan area of 400 m $\times$ 400 m and a scan depth of 50 m. The remaining parameters were fixed as follows: sonar horizontal beamwidth of 130°, vertical beamwidth of 20°, ROV cruising speed of 1.5 m/s, turning speed of 10°/s, and diving speed of 0.25 m/s. The sonar detection range was varied from 10 m to 100 m in increments of 10 m.

The simulation results, summarized in Table 7, show that the total mission duration generally decreases as the sonar detection range increases. This trend reflects the reduced number of required scan paths and scanning layers enabled by larger detection ranges. For sonar detection ranges between 50 m and 100 m, the total mission duration remains within the assumed upper limit of 1.5 h, indicating that the zigzag pattern maintains operational feasibility for rectangular scan areas under these conditions.

Table 7. Simulated total mission durations for zigzag path planning in rectangular scan areas.

Sonar Detection Range (m)	Total Mission Duration (Hour)
100	0.59
90	0.60
80	0.60
70	0.76
60	0.76
50	1.40
40	1.63
30	2.82
20	6.14
10	22.72

3.1.5. Summary of Path Planning Methods

Based on the comparative results summarized in Table 8, the relative effectiveness of the proposed path planning methods can be consolidated for both circular and rectangular scan geometries:

- For circular scan areas, the zigzag-II and arithmetic spiral-III patterns demonstrate the most favorable performance, achieving reduced mission duration while preserving complete volumetric coverage across a wide range of sonar detection ranges.
- For rectangular scan areas, the zigzag pattern consistently yields the shortest mission duration under the evaluated parameter settings, indicating its robustness when extended from circular to rectangular scan geometries.

Table 8. Summary of simulation results for zigzag-based planning in rectangular scan areas and zigzag-II and spiral-III planning in circular scan areas.

Single Planar Layer Path Length	Total Mission Duration (Hour)		
	Circular Scan Area		Rectangular Scan Area
	Zigzag-II	Arithmetic Spiral-III	Zigzag
100	0.52	0.50	0.59
90	0.53	0.52	0.60
80	0.53	0.54	0.60
70	0.64	0.58	0.76
60	0.66	0.63	0.76
50	1.19	1.13	1.40
40	1.40	1.31	1.63
30	2.38	2.21	2.82
20	5.07	4.71	6.14
10	18.97	17.81	22.72

3.2. Path Coverage Issues Observed in Simulation

The paths generated by the MATLAB-based graphical user interface are imported into the OpenGL-based ROV animation interface for visualization. For circular scan areas, the simulated path patterns include the zigzag-II and arithmetic spiral-III patterns, while for rectangular scan areas, the zigzag pattern is used. The simulation parameters are fixed across all cases to facilitate consistent comparison. Specifically, the sonar detection range is set to 100 m, with a horizontal beamwidth of 130° and a vertical beamwidth of 20°. The circular scan area has a radius of 200 m, and the rectangular scan area measures 400 m × 400 m, with both areas having a scanning depth of 50 m. The ROV's cruising speed is set to 3 knots, the turning rate to 10°/s, and the diving speed to 0.25 m/s. A single

simulated mine is placed at coordinates (200, 220, 30) meters to provide a reference target for visualization.

The simulation results reveal several pattern-specific coverage issues that depend on both scan area geometry and path strategy. For the zigzag-II pattern applied to circular scan areas, unscanned regions consistently appear near the start and end of each horizontal path within a single layer. These gaps become more pronounced in the lower scan layers, where the effects of sonar beam geometry accumulate across depth transitions. In rectangular scan areas, the zigzag pattern exhibits unscanned regions near the bottom edges of the scan volume, particularly at the start of each horizontal path. For the arithmetic spiral-III pattern, which is applied only to circular scan areas, a coverage issue arises when the scan direction transitions between inward and outward spirals in the second layer, leaving a portion of the central region insufficiently covered. Collectively, these observations indicate that while the evaluated path planning methods achieve broad volumetric coverage, localized gaps remain near path boundaries and layer transitions, motivating further refinement of the planning rules.

One underlying cause of the observed coverage gaps in the lower scan layers is the sonar's fixed tilt angle, which introduces a blind zone at the bottom of each scanning layer. As illustrated in Figure 27, this unscanned gap—denoted by h_f—arises from the downward inclination of the sonar beam relative to the horizontal plane. For a sonar detection range $R = 100$ m, a vertical beamwidth $\phi = 20°$, and a tilt angle $\psi = 15°$, the length of this blind zone is calculated as 90.63 m using Equation (18):

$$h_f = R \times \cos\left(\frac{\phi}{2} + \psi\right) \tag{18}$$

where h_f is the unscanned bottom gap length; R is the sonar detection range; ϕ is the vertical beamwidth; and ψ is the sonar inclination angle.

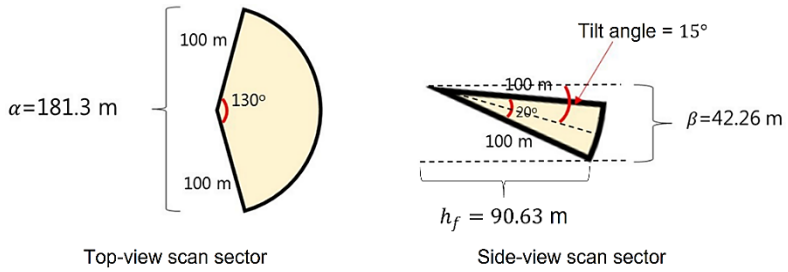

Figure 27. Schematic of sonar bottom gap caused by inclined beam geometry.

3.3. Corrected Path Planning Strategies

- Correction of Initial and Terminal Path Gaps in Single-Layer Scans
  1. For the zigzag pattern in rectangular scan areas and the zigzag-II pattern in circular scan areas, unscanned regions consistently appear near the starting point of each horizontal path segment due to the sonar's inclined beam geometry. This configuration creates a near-field blind zone directly beneath the sonar at the beginning of each horizontal scan line. To eliminate this coverage gap, the initial position of each horizontal path segment is extended by a fixed distance h_f, which is determined from the sonar detection range, tilt angle, and vertical beamwidth using Equation (18).
  2. In circular scan areas, the zigzag-II pattern further exhibits unscanned regions at the starting and terminal points of a single-layer scan path. This issue arises because the overall horizontal extent of the planned trajectory is insufficient to fully cover the circular boundary at the beginning and end of the layer. To correct

this limitation, the single-layer path is extended by distances h_s and h_e at the starting and ending positions, respectively, as illustrated in Figure 28. Here, h_s represents the horizontal distance required to extend the path from the initial scan endpoint to the circular boundary, while h_e denotes the corresponding extension at the terminal endpoint. These adjustments ensure complete boundary coverage at both ends of the scan layer while preserving the original scan spacing and interior coverage characteristics.

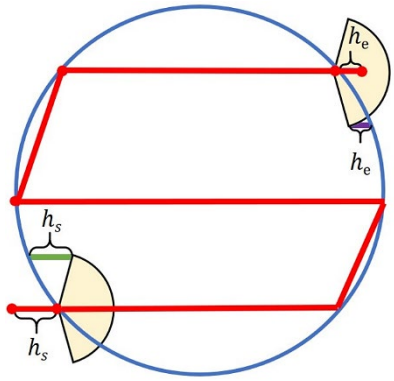

Figure 28. Correction of initial and terminal gaps in a single-layer zigzag-II scan path for a circular scan area by extending the path endpoints.

- Adjustment Based on Vertical-Distance-Dependent Sonar Coverage
  To address unscanned regions that arise within a single planar scan layer as the scan plane approaches the bottom of the sonar coverage volume, this study analyzes how the geometric characteristics of sonar coverage vary with vertical distance from the sonar. These issues manifest differently depending on scan geometry and path pattern. For rectangular scan areas, the zigzag pattern exhibits unscanned regions near the periphery of the scan area when the planar layer is located closer to the bottom of the sonar scan cone. For circular scan areas, the zigzag-II pattern experiences insufficient overlap between adjacent horizontal paths within a single layer, resulting in unscanned gaps between paths as the vertical distance from the sonar increases.
  To quantitatively characterize this behavior, the relationship between the sonar top-view scan sector chord length (α) and the vertical distance (γ) is examined. A curve-fitting model is employed to approximate how α varies as a function of γ. As illustrated in Figure 29, the chord length α decreases monotonically with increasing vertical distance γ, reflecting the contraction of the sonar's effective horizontal coverage at larger offsets from the sonar.

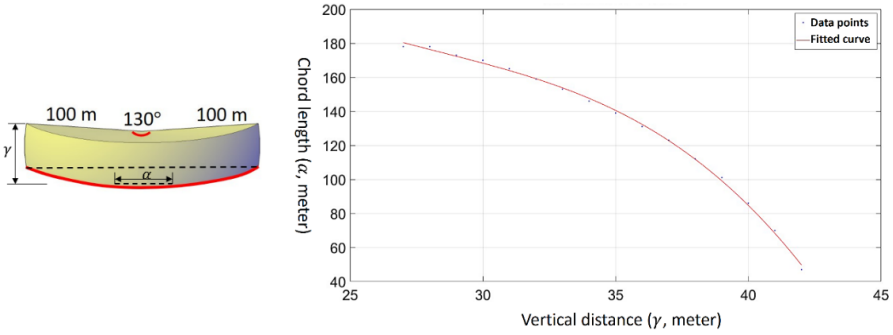

Figure 29. Curve-fitted relationship between the top-view sonar sector chord length (α) and vertical distance (γ).

The first-order derivative of the fitted function $\alpha(\gamma)$ with respect to γ is then computed to assess the rate at which the chord length changes with vertical distance, as shown in Figure 30. The magnitude of the derivative increases with γ, indicating that variations in horizontal coverage become more pronounced as the scan plane approaches the lower boundary of the sonar scan cone.

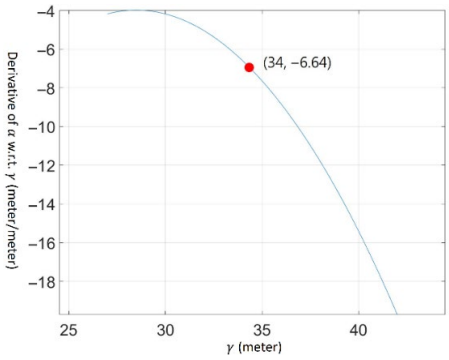

Figure 30. First-order derivative of the chord length function $\alpha(\gamma)$ with respect to vertical distance, indicating the rate of change in horizontal sonar coverage.

To determine an appropriate vertical distance for adjusting the chord length used in path planning, the vertical distance corresponding to the median value of the derivative magnitude is selected. This vertical distance is defined as γ_1, and the corresponding chord length is denoted as $\alpha\prime$. In addition, the vertical distance at the bottom edge of the sonar scan cone is defined as γ_2, with its associated chord length denoted as α. These parameters are illustrated in Figure 31.

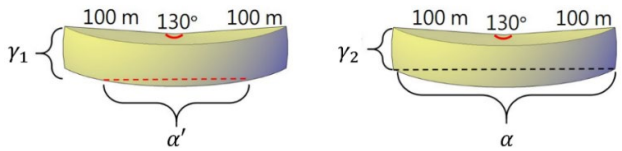

Figure 31. Definition of γ_1 and γ_2, corresponding to the median-derivative location and the bottom edge of the sonar scan cone, along with their associated chord lengths α' and α.

Based on γ_1 and γ_2, a vertical-distance-dependent decision rule is proposed to determine the chord lengths used in the final two scanning layers of the planned trajectory. The rule is defined as follows:

1. If the remaining vertical distance is $\leq 2\gamma_1$ and $> (\gamma_1 + \gamma_2)$, assign α ' to both layers.
2. If the remaining vertical distance is $\leq (\gamma_1 + \gamma_2)$ and $> 2\gamma_2$, assign α' to the upper layer and α to the lower layer.
3. If the remaining vertical distance is $\leq 2\gamma_2$, assign α to both layers.

- Revised Path Planning Schemes
  Following the corrections described above, updated path layouts have been implemented. The corrected zigzag path for a rectangular scan area and the corrected zigzag-II path for a circular scan area are presented in Figures 32 and 33, respectively. In the following figures, the term "corrected" refers to the incorporation of the gap-compensation rules derived in the preceding sections, while the underlying path topology remains unchanged.

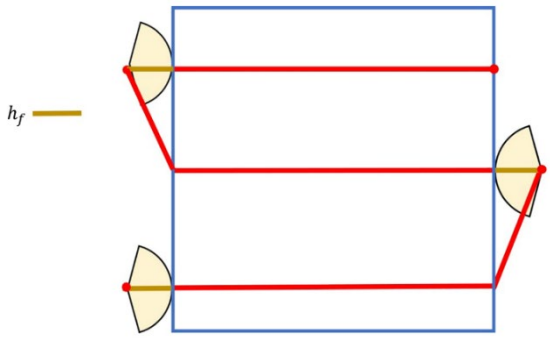

Figure 32. Corrected zigzag path in a rectangular scan area.

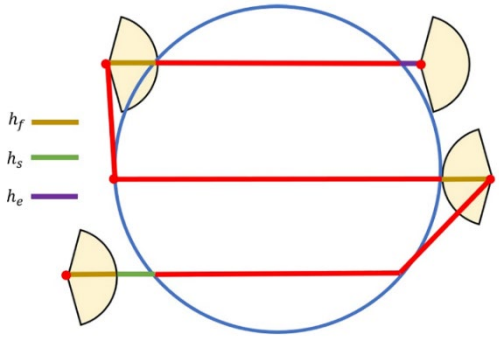

Figure 33. Corrected zigzag-II path in a circular scan area.

For the arithmetic spiral-III pattern applied to circular scan areas, a coverage gap was observed near the central region during outward execution of the second-layer scan path. To mitigate this issue, the starting point is shifted inward by a distance h_f, as illustrated in Figure 34 and determined using Equation (18).

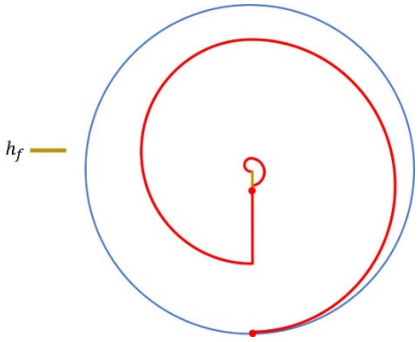

Figure 34. Corrected arithmetic spiral-III path in a circular scan area.

3.4. Simulation Results of Corrected Path Planning Patterns

- Validation of 3D Water Area Coverage

  This section presents simulation results for the corrected (gap-compensated) path planning algorithms introduced in Section 3.3, visualized using the OpenGL-based ROV animation interface. The evaluated path patterns include: (1) the corrected zigzag pattern for rectangular scan areas; (2) the corrected zigzag-II pattern for circular scan areas; and (3) the corrected arithmetic spiral-III pattern for circular scan areas.

  The simulation parameters are as follows: the sonar detection range is 100 m, with a horizontal beamwidth of 130° and a vertical beamwidth of 20°. The circular scan area has a radius of 200 m, while the rectangular scan area measures 400 m × 400 m. The scanning depth for both configurations is 50 m. The ROV is simulated with a cruising speed of 1.5 m/s, a turning rate of 10°/s, and a diving speed of 0.25 m/s. A

simulated mine is placed at coordinates (200, 220, 30) in meters. Simulation results for the three corrected path planning methods are shown in Figures 35–37. These results visually demonstrate that the proposed improvements eliminate the previously identified coverage gaps and enable complete geometric coverage of the designated 3D scan area under the assumed idealized conditions.

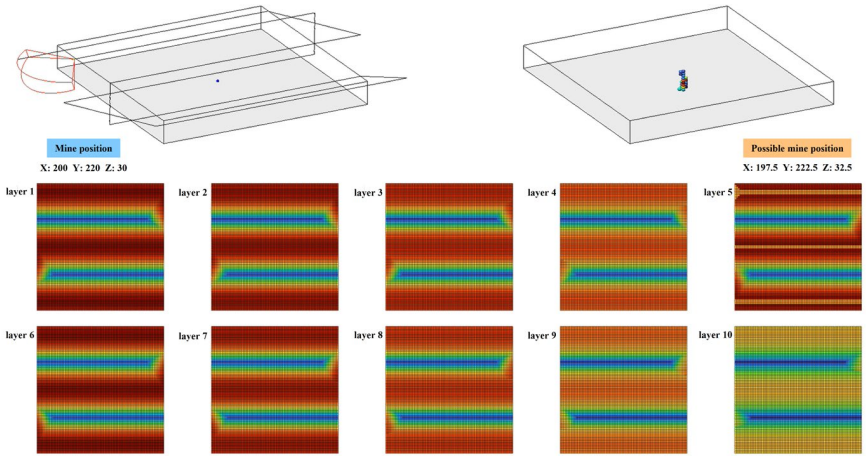

Figure 35. Simulation result of the corrected zigzag pattern in a rectangular scan area. Dark red indicates the maximum value and dark blue the minimum value.

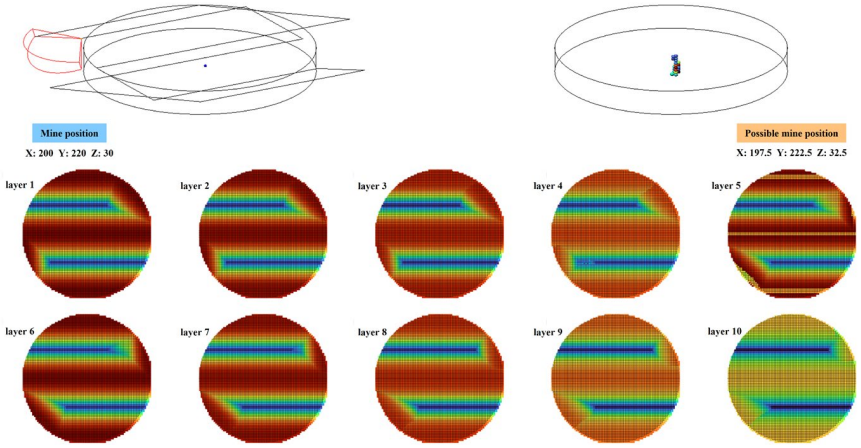

Figure 36. Simulation result of the corrected zigzag-II pattern in a circular scan area. Dark red indicates the maximum value and dark blue the minimum value.

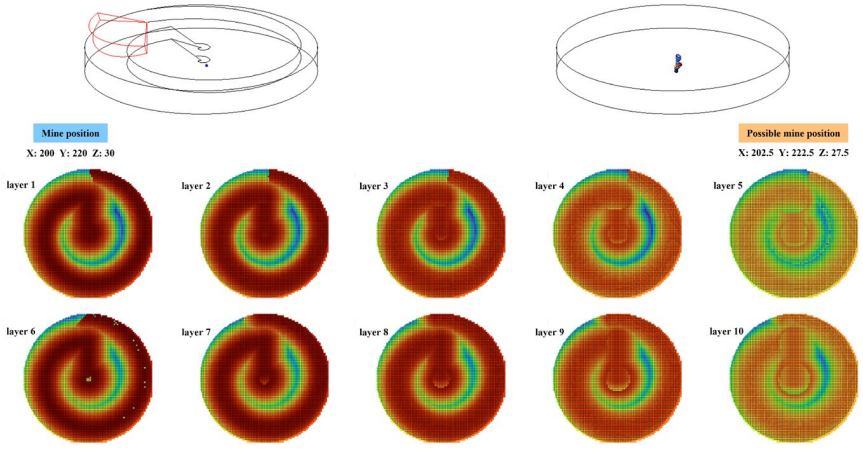

Figure 37. Simulation result of the corrected arithmetic spiral-III pattern in a circular scan area. Dark red indicates the maximum value and dark blue the minimum value.

- Target Localization Evaluation
  To evaluate localization performance under idealized sensing assumptions, a simulated mine was placed within the scan areas at the following five coordinates: (178, 221, 9), (251, 14, 27), (129, 278, 14), (218, 125, 22), and (267, 213, 32). The ROV animation interface records the sonar coverage and estimates positional errors in the x, y, and z directions. Simulation results show that:
  1. For the corrected zigzag-II pattern in the circular scan area, x-axis and y-axis errors are all less than 2.5 m, and z-axis errors range from 0.5 m to 11.5 m, as illustrated in Figure 38;
  2. For the corrected arithmetic spiral-III pattern, x-axis and y-axis errors remain under 2.5 m, while z-axis errors range from 0.5 m to 14.5 m, as illustrated in Figure 39;
  3. For the corrected zigzag pattern in the rectangular scan area, x-axis and y-axis errors are below 2.5 m, and z-axis errors range from 1.5 m to 4.5 m, as illustrated in Figure 40.

  These results indicate that, under idealized sensing and motion assumptions, the corrected path planning algorithms can support consistent target localization with bounded spatial error within the scanned volume.

- Simulation Across Multiple Sonar Ranges
  To further evaluate the behavior of the corrected path planning methods under varying sensing conditions, simulations were conducted using sonar detection ranges from 10 m to 100 m in 10 m increments. The evaluated configurations include:
  1. Circular scan area: radius 200 m, scan depth 50 m, using the corrected zigzag-II and arithmetic spiral-III patterns;
  2. Rectangular scan area: 400 m $\times$ 400 m, scan depth 50 m, using the corrected zigzag pattern;
  3. Multibeam forward-looking sonar: 130° horizontal beamwidth and 20° vertical beamwidth;
  4. ROV motion parameters: cruising speed 1.5 m/s, turning rate 10°/s, and diving speed 0.25 m/s.

All simulations are performed under the same idealized assumptions, allowing the influence of sonar detection range on mission duration to be examined in isolation.

The simulation results, summarized in Table 9, show that mission duration generally decreases as sonar detection range increases for all corrected path planning methods. For circular scan areas, the corrected zigzag-II pattern requires 3.55 h at a detection range of 30 m, compared to 3.79 h for the corrected arithmetic spiral-III pattern. For all other evaluated ranges, the corrected arithmetic spiral-III pattern yields shorter mission durations than the corrected zigzag-II pattern. When the sonar detection range is between 50 m and 100 m, both corrected circular-area patterns satisfy the assumed 1.5 h mission time constraint. For rectangular scan areas, the corrected zigzag pattern remains within the same mission time limit when the sonar detection range is between 60 m and 100 m. These trends highlight the sensitivity of volumetric scan efficiency to sonar detection range and demonstrate the effectiveness of the proposed corrections across both scan geometries.

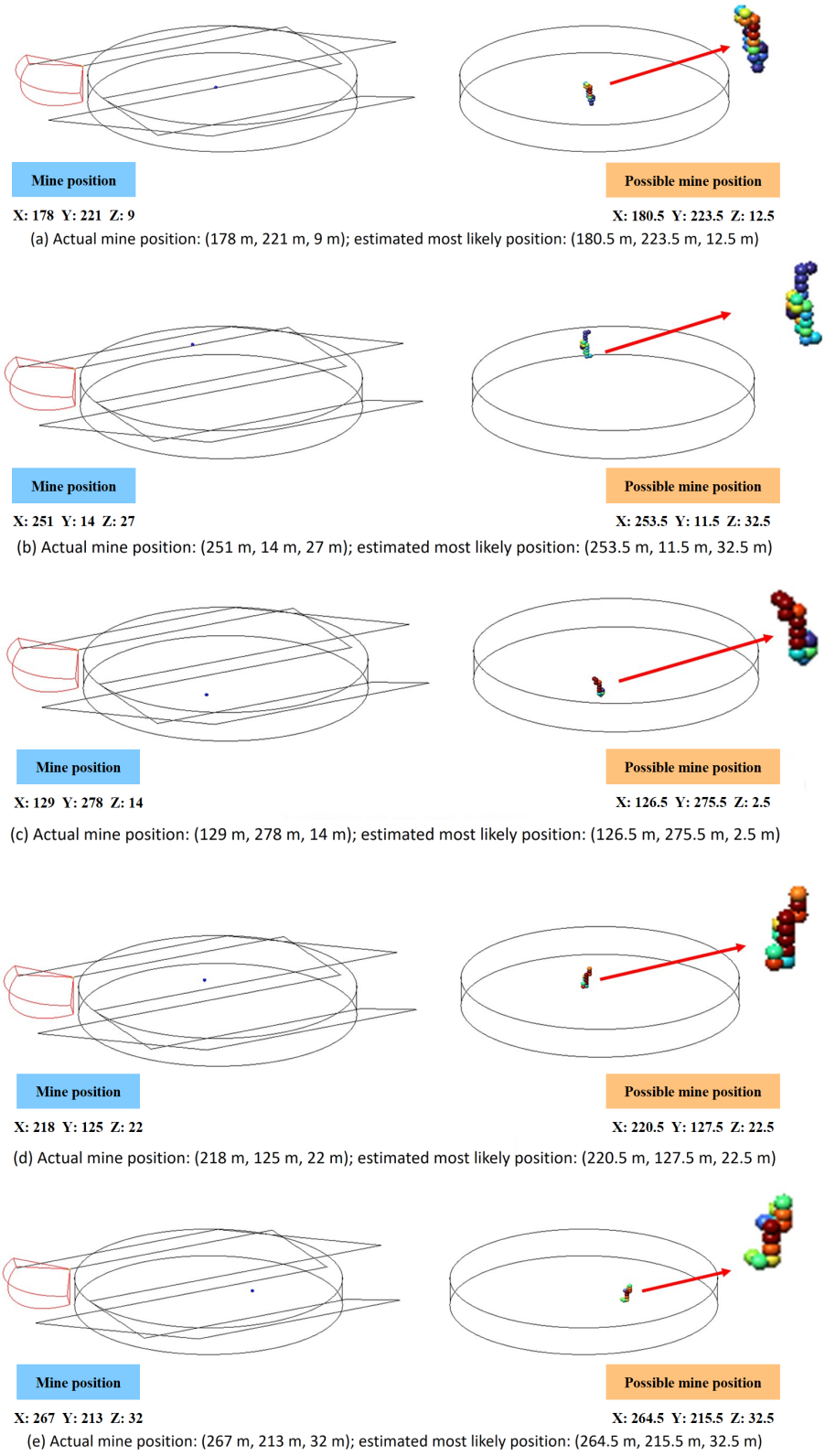

Figure 38. Estimated mine locations using the corrected zigzag-II pattern in a circular scan area for different target placements (**a**–**e**). Dark red indicates the maximum value and dark blue the minimum value.

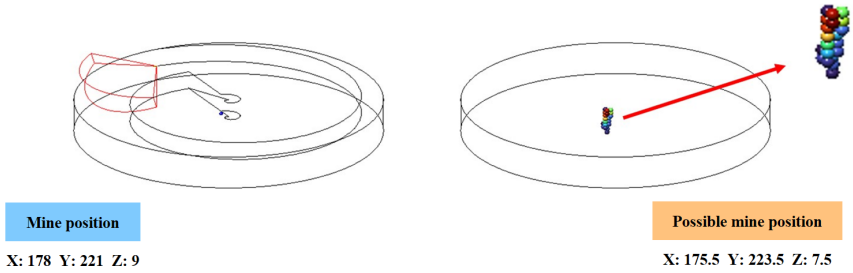

(a) Actual mine position: (178 m, 221 m, 9 m); estimated most likely position: (175.5 m, 223.5 m, 7.5 m)

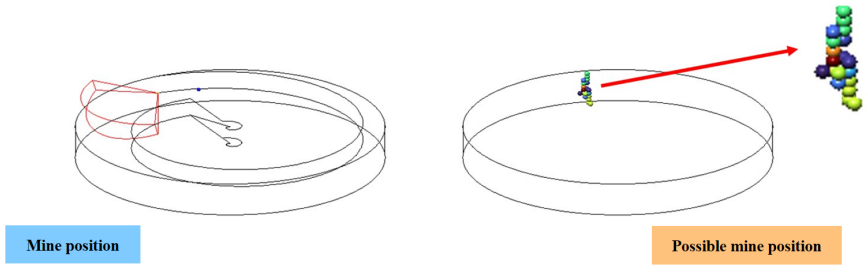

(b) Actual mine position: (251 m, 14 m, 27 m); estimated most likely position: (248.5 m, 11.5 m, 27.5 m)

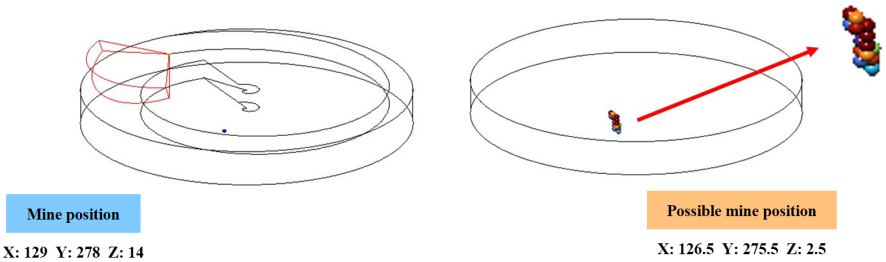

(c) Actual mine position: (129 m, 278 m, 14 m); estimated most likely position: (126.5 m, 275.5 m, 2.5 m)

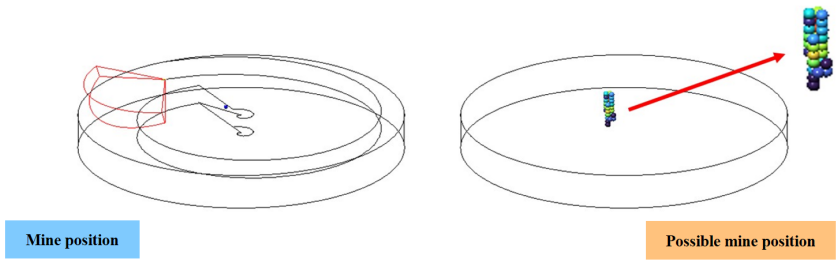

(d) Actual mine position: (218 m, 125 m, 22 m); estimated most likely position: (220.5 m, 122.5 m, 7.5 m)

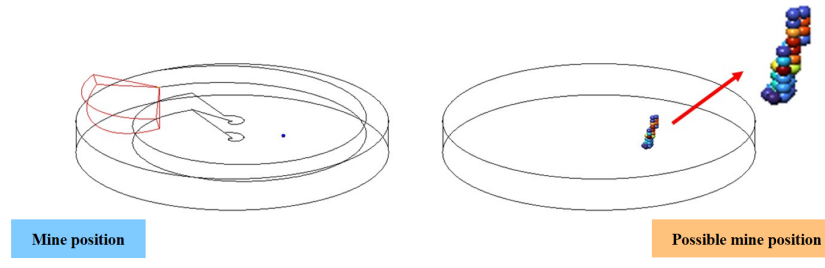

(e) Actual mine position: (267 m, 213 m, 32 m); estimated most likely position: (264.5 m, 215.5 m, 32.5 m)

Figure 39. Estimated mine locations using the corrected arithmetic spiral-III pattern in a circular scan area for different target placements (**a**–**e**). Dark red indicates the maximum value and dark blue the minimum value.

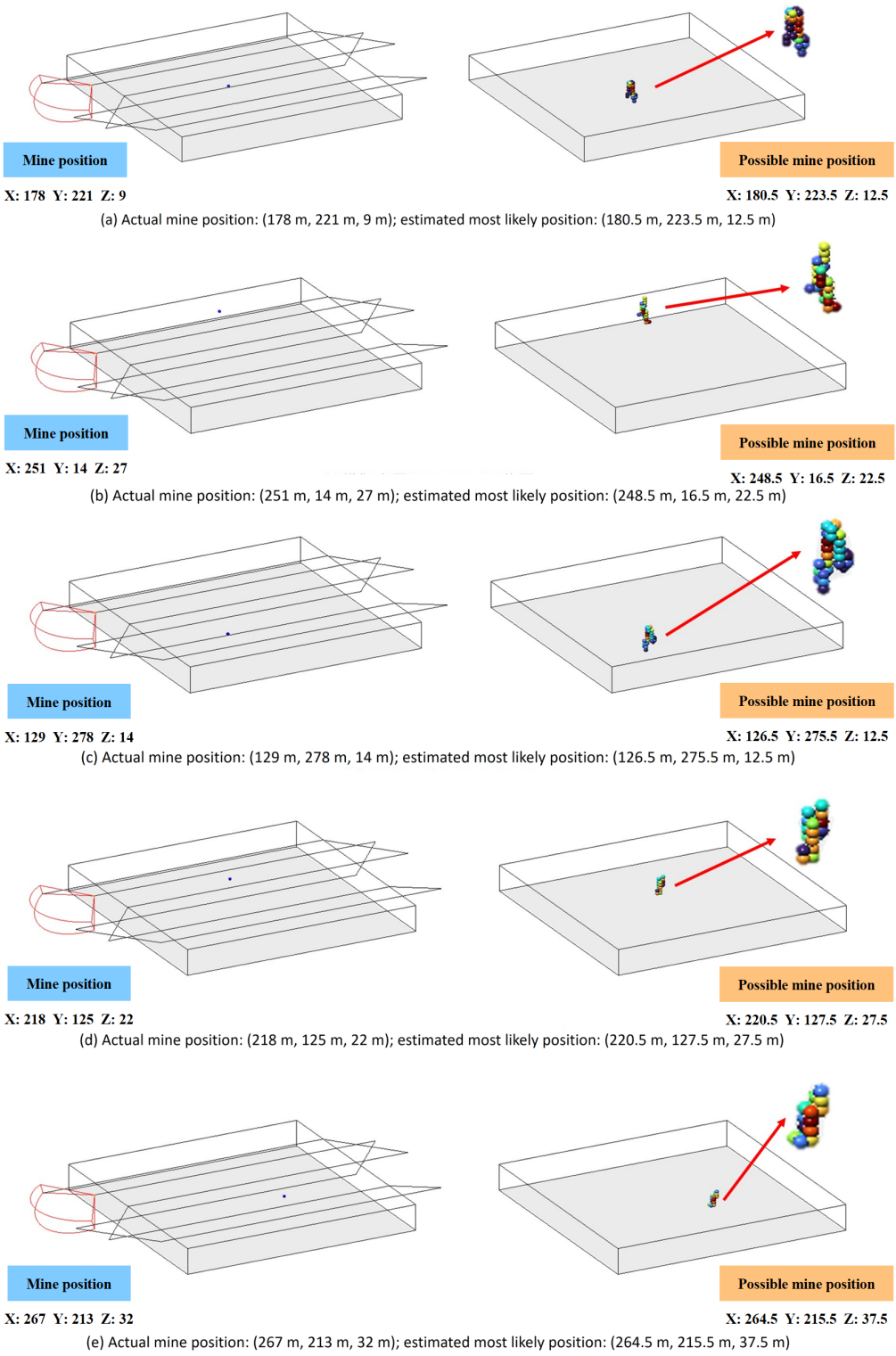

Figure 40. Estimated mine locations using the corrected zigzag pattern in a rectangular scan area for different target placements (**a**–**e**). Dark red indicates the maximum value and dark blue the minimum value.

Table 9. Mission duration of corrected path planning methods under varying sonar detection ranges for circular and rectangular scan areas.

Sonar Detection Range (m)	Total Mission Duration (Hour)		
	Circular Scan Area		Rectangular Scan Area
	Corrected Zigzag-II	Corrected Arithmetic Spiral-III	Corrected Zigzag
100	0.63	0.46	0.70
90	0.64	0.76	0.70
80	0.94	0.80	1.02
70	1.26	0.85	1.48
60	1.27	1.24	1.49
50	1.56	1.46	1.83
40	2.63	2.13	2.96
30	3.55	3.79	4.22
20	7.92	7.76	9.61
10	39.43	35.80	48.70

3.5. Discussion

This study investigates volumetric scan path planning from a deterministic and geometry-driven perspective, with emphasis on guaranteeing full three-dimensional coverage under bounded mission duration. The discussion below contextualizes the observed simulation results by examining the causes of coverage gaps, the effectiveness of the proposed corrections, the limitations of idealized simulation assumptions, and the relationship between the present approach and existing underwater survey and mapping methodologies.

3.5.1. Origins of Coverage Gaps in Volumetric Scanning

The simulation results reveal that coverage gaps arise primarily from geometric interactions between sonar beam characteristics and scan path construction, rather than from execution or control deficiencies. Specifically, blind zones and unscanned regions occur near path boundaries, at layer transitions, and in lower scan layers where the effective horizontal footprint of the sonar contracts with increasing vertical distance from the sensor. These effects are inherent to forward-looking multibeam sonar geometry and cannot be eliminated through planar coverage logic alone.

Similar geometric sensitivities have been observed in large-scale underwater survey missions, where scan effectiveness depends strongly on sensor footprint, altitude, and trajectory spacing. For example, Yoerger et al. [12] demonstrated that nested and layered survey trajectories are essential for achieving reliable near-bottom coverage in deep-sea environments, implicitly highlighting the need to account for three-dimensional sensing geometry during path design. The present study extends this insight by explicitly diagnosing how such geometric effects manifest as localized coverage gaps in volumetric scan planning.

3.5.2. Effectiveness of Deterministic Geometric Corrections

The corrected path planning strategies proposed in this work address these coverage gaps through deterministic, rule-based modifications derived directly from sonar beam geometry. Adjustments such as near-field gap compensation, boundary extension, and vertical-distance-dependent chord length selection enable consistent overlap between adjacent scan paths and layers without introducing additional control complexity.

This geometry-driven correction philosophy contrasts with approaches that rely on feedback from localization or mapping uncertainty. For instance, vision-based inspec-

tion systems, such as the ROV stereovision framework presented by Negahdaripour and Firoozfam [16], emphasize accurate pose estimation and sensor fusion to support inspection coverage. While effective for close-range visual inspection, such methods depend on feature visibility and localization quality. In contrast, the present study demonstrates that systematic geometric reasoning alone can significantly improve volumetric coverage when sensing is dominated by forward-looking sonar.

3.5.3. Limitations of Idealized Simulation Assumptions

All simulations in this study are conducted under idealized, disturbance-free assumptions to isolate geometric coverage behavior. As a result, factors such as navigation drift, sensor noise, and environmental disturbances are intentionally excluded. In practical deployments, these effects are commonly addressed through SLAM-based estimation or post-processing techniques. For example, Barkby et al. [17] and Pizarro et al. [18] demonstrated how bathymetric SLAM and large-scale optical reconstruction can compensate for navigation uncertainty during extended survey missions.

While such methods enhance localization accuracy and map consistency, they do not replace the need for geometrically sound scan planning. In fact, poorly designed trajectories may still lead to systematic coverage gaps even when advanced estimation techniques are applied. The present work therefore positions deterministic volumetric scan planning as a complementary baseline, upon which estimation-based or learning-based methods may later build.

3.5.4. Positioning Relative to Existing Underwater Survey Approaches

Compared to prior work emphasizing adaptive planning, mapping accuracy, or real-time reconstruction, the primary contribution of this study lies in its explicit treatment of volumetric scan completeness under known sensing geometry. The layered scan framework and correction rules are designed to ensure that the entire pre-defined scan volume is systematically traversed within a bounded mission duration.

Large-area reconstruction approaches, such as those reported by Pizarro et al. [18], demonstrate the value of post-mission data integration for producing detailed three-dimensional representations. However, their effectiveness pre-supposes sufficient data coverage. The present study addresses this prerequisite by focusing on pre-mission trajectory design that guarantees coverage integrity, particularly for missions involving the detection of isolated midwater or moored objects.

Overall, the results suggest that geometry-driven volumetric scan planning provides a transparent and analytically grounded foundation for underwater search missions using forward-looking sonar. Future extensions may incorporate environmental disturbances, vehicle control uncertainty, or adaptive decision-making, while preserving the geometric principles established in this work.

4. Conclusions

This study presented a deterministic, geometry-driven framework for volumetric path planning for three-dimensional underwater scanning using a forward-looking sonar-equipped ROV. The main contributions and findings are summarized as follows:

- Geometry-driven volumetric planning:
  A unified analytical framework was developed to construct layered scan trajectories directly from sonar detection range, beam geometry, and scan volume dimensions, enabling transparent estimation of path length and mission duration.
- Identification and correction of coverage failure modes:
  Systematic analysis revealed non-obvious coverage gaps and non-monotonic perfor-

mance trends arising from sonar beam inclination, boundary truncation, and vertical-distance-dependent chord contraction. These effects were explicitly diagnosed and resolved through deterministic, rule-based corrections.

- Validated corrected scan strategies:
  Under idealized simulation conditions, the corrected zigzag pattern for rectangular scan areas and the corrected zigzag-II and arithmetic spiral-III patterns for circular scan areas achieved complete volumetric coverage with bounded mission duration and consistent localization accuracy across a range of sonar detection ranges.
- Practical implications for tethered ROV operation:
  For rectangular scan areas, the corrected zigzag pattern offers reliable coverage with simple trajectory structure and predictable motion. For circular scan areas, while both corrected zigzag-II and arithmetic spiral-III patterns achieve full coverage, the corrected zigzag-II pattern is more robust for tethered operations due to reduced cable management complexity.
- Scope and future work:
  The proposed framework serves as a baseline analytical reference for volumetric scan planning. Future work may incorporate environmental disturbances, vehicle control uncertainty, or adaptive and learning-based extensions while preserving the geometric foundations established in this study.

Author Contributions: Conceptualization, Y.-C.C.; methodology, Y.-C.C.; software, Y.-C.C. and W.-S.C.; validation, Y.-C.C. and W.-S.C.; formal analysis, Y.-C.C. and W.-S.C.; investigation, Y.-C.C. and W.-S.C.; resources, Y.-C.C.; data curation, Y.-C.C. and W.-S.C.; writing—original draft preparation, Y.-C.C. and W.-S.C.; writing—review and editing, Y.-C.C.; visualization, Y.-C.C. and W.-S.C.; supervision, Y.-C.C.; project administration, Y.-C.C.; funding acquisition, Y.-C.C. All authors have read and agreed to the published version of the manuscript.

Funding: This research was funded by the National Science and Technology Council (NSTC) of Taiwan under grant number NSTC 114-2221-E-110-041.

Data Availability Statement: All data are available from the corresponding author upon reasonable request and are not publicly available due to ongoing studies.

Conflicts of Interest: The authors declare no conflict of interest.

References

1. Bellingham, J.G.; Rajan, K. Robotics in remote and hostile environments. *Science* **2007**, *318*, 1098–1102. [CrossRef] [PubMed]
2. Galceran, E.; Carreras, M. A survey on coverage path planning for robotics. *Robot. Auton. Syst.* **2013**, *61*, 1258–1276. [CrossRef]
3. Goh, Y.; Fan, S. Path planning for AUV area coverage mission based on MOOS-IvP. In Proceedings of the 2019 IEEE Underwater Technology (UT), Kaohsiung, Taiwan, 16–19 April 2019; pp. 1–10.
4. Cardaillac, A.; Ludvigsen, M. Path following for underwater inspection allowing manoeuvring constraints. In Proceedings of the International Conference on Intelligent Autonomous Systems, Zagreb, Croatia, 13–16 June 2022; pp. 867–880.
5. Shi, J.; Zhou, M. A data-driven intermittent online coverage path planning method for AUV-based bathymetric mapping. *Appl. Sci.* **2020**, *10*, 6688. [CrossRef]
6. Wang, J.; Tang, Y.; Jin, S.; Bian, G.; Zhao, X.; Peng, C. A method for multi-beam bathymetric surveys in unfamiliar waters based on the AUV constant-depth mode. *J. Mar. Sci. Eng.* **2023**, *11*, 1466. [CrossRef]
7. Tang, Y.; Wang, L.; Jin, S.; Zhao, J.; Huang, C.; Yu, Y. AUV-based side-scan sonar real-time method for underwater-target detection. *J. Mar. Sci. Eng.* **2023**, *11*, 690. [CrossRef]
8. Masmitja, I.; Martin, M.; Katija, K.; Gomariz, S.; Navarro, J. A reinforcement learning path planning approach for range-only underwater target localization with autonomous vehicles. In Proceedings of the 2022 IEEE 18th International Conference on Automation Science and Engineering (CASE), Mexico City, Mexico, 20–24 August 2022; pp. 675–682.
9. Mane, P.; George, A.J.; Makam, R.; Majumder, R.; Sundaram, S. EROAS: 3D efficient reactive obstacle avoidance system for autonomous underwater vehicles using 2.5 D forward-looking sonar. *arXiv* **2024**, arXiv:2411.05516.

10. Cheng, C.; Wang, C.; Yang, D.; Liu, W.; Zhang, F. Underwater localization and mapping based on multi-beam forward looking sonar. *Front. Neurorobot.* **2022**, *15*, 801956. [CrossRef] [PubMed]
11. Zhang, J.; Xie, Y.; Ling, L.; Folkesson, J. A fully-automatic side-scan sonar simultaneous localization and mapping framework. *IET Radar Sonar Navig.* **2024**, *18*, 674–683. [CrossRef]
12. Yoerger, D.R.; Jakuba, M.; Bradley, A.M.; Bingham, B. Techniques for deep sea near bottom survey using an autonomous underwater vehicle. *Int. J. Robot. Res.* **2007**, *26*, 41–54. [CrossRef]
13. Chou, Y.-C.; Chang, W.-S.; Chen, H.-H.; Wang, C.-C. A preliminary study of forward-looking sonar based path planning for remotely operated vehicles. In Proceedings of the 2025 IEEE Underwater Technology (UT), Taipei, Taiwan, 2–5 March 2025; pp. 1–4.
14. Blueprint Subsea: Oculus M-Series Multibeam Imaging Sonars. Available online: https://www.blueprintsubsea.com/oculus/oculus-m-series (accessed on 3 February 2026).
15. Exail: Seascan-M ROV for Subsea Insepction and Identification. Available online: https://www.exail.com/product/seascan-mine-identification-system (accessed on 3 February 2026).
16. Negahdaripour, S.; Firoozfam, P. An ROV stereovision system for ship-hull inspection. *IEEE J. Ocean. Eng.* **2007**, *31*, 551–564. [CrossRef]
17. Barkby, S.; Williams, S.B.; Pizarro, O.; Jakuba, M.V. A featureless approach to efficient bathymetric SLAM using distributed particle mapping. *J. Field Robot.* **2011**, *28*, 19–39. [CrossRef]
18. Pizarro, O.; Eustice, R.M.; Singh, H. Large area 3-D reconstructions from underwater optical surveys. *IEEE J. Ocean. Eng.* **2009**, *34*, 150–169. [CrossRef]